Article:
Croft, H., Chen, J.M., Wang, R. et al. (2020) The global distribution of leaf chlorophyll content. Remote Sensing of Environment, 236. 111479. ISSN: 0034-4257

https://doi.org/10.1016/j.rse.2019.111479

The global distribution of leaf chlorophyll content

Croft, H.[ab]*Chen, J.M.[a] Wang, R.[a] Mo, G.[a] Luo, S.[c] Luo, X.[d] He, L.[a] Gonsamo, A.[a] Arabian, J.[ae]

Zhang, Y. [f] Simic-Milas, A.[g] Noland, T.L.[h] He, Y.[i] Homolová, L.[j] Malenovský, Z.[jk] Yi, Q.[l] Beringer, J.[m]

Amiri, R.[n] Hutley, L.[o] Arellano, P.[p] Stahl, C.[q] Bonal, D.[r]

[a] *University of Toronto, Department of Geography, Toronto, ON M5S 3G3, Canada*

**holly.croft@utoronto.ca*

[b] *University of Sheffield, Department of Animal and Plant Sciences, Sheffield, S10 2TN, U.K.*

[c] *Key Laboratory of Digital Earth Science, Institute of Remote Sensing and Digital Earth, Chinese Academy of Sciences, Beijing 100094, China*

[d] *Lawrence Berkeley National Laboratory, Climate and Ecosystem Sciences Division, Berkeley, CA 94720, USA*

[e] *WWF-Canada, 410 Adelaide Street W, Toronto, ON M5V 1S8, Canada*

[f] *Delta State University, Division of Biological and Physical Sciences, Cleveland, MS 38733, USA*

[g] *Bowling Green State University, Department of Geology, Bowling Green, OH 43403-0211, USA*

[h] *Ontario Ministry of Natural Resources, Ontario Forest Research Institute, 1235 Queen St. E., Sault Ste. Marie, ON P6A 2E5 Canada*

[i] *University of Toronto Mississauga, Department of Geography, 3359 Mississauga Rd, Mississauga, ON L5L 1C6, Canada*

[j] *Global Change Research Institute CAS, Bělidla 986/4a, Brno 603 00, Czech Republic*

[k] *University of Tasmania, School of Land and Food, Surveying and Spatial Sciences Group, Private Bag 76, Hobart, TAS 7001, Australia*

[l] *Xinjiang Institute of Ecology and Geography Chinese Academy of Sciences, 818 Beijing South Road, Urumqi, Xinjiang 830011, PR China*

[m] *The University of Western Australia, School of Earth and Environment (SEE), Crawley WA, 6009, Australia*

[n] *Monash University, School of Earth, Atmosphere and Environment, Clayton VIC, 3800, Australia*

[o] *Charles Darwin University, School of Environment, Research Institute for the Environment and Livelihoods, NT 0909, Australia*

[p] *Yachay Tech University, School of Geological Sciences and Engineering, Center of Earth Observation (CEO), Urcuqui, Ecuador*

[q] *INRA, UMR Ecologie des Forêts de Guyane, Campus Agronomique, BP 709, 97387 Kourou Cedex, French Guiana*

[r] *UMR EEF, INRA Université de Lorraine, 54280 Champenoux, France*

Abstract

Leaf chlorophyll is central to the exchange of carbon, water and energy between the biosphere and the atmosphere, and to the functioning of terrestrial ecosystems. This paper presents the first spatially continuous view of terrestrial leaf chlorophyll content (Chl_{Leaf}) across a global scale. Weekly maps of Chl_{Leaf} were produced from ENIVSAT MERIS full resolution (300 m) satellite data with a two-stage physically-based radiative transfer modelling approach. Firstly, leaf-level reflectance was derived from top-of-canopy satellite reflectance observations using 4-Scale and SAIL canopy radiative transfer models

for woody and non-woody vegetation, respectively. Secondly, the modelled leaf-level reflectance was used in the PROSPECT leaf-level radiative transfer model to derive Chl_{Leaf}. The Chl_{Leaf} retrieval algorithm was validated with measured Chl_{Leaf} data from 248 sample measurements at 28 field locations, and covering six plant functional types (PFTs). Modelled results show strong relationships with field measurements, particularly for deciduous broadleaf forests (R^2 = 0.67; RMSE = 9.25 μg cm^{-2}; p<0.001), croplands (R^2 = 0.41; RMSE = 13.18 μg cm^{-2}; p<0.001) and evergreen needleleaf forests (R^2 = 0.47; RMSE = 10.63 μg cm^{-2}; p<0.001). When the modelled results from all PFTs were considered together, the overall relationship with measured Chl_{Leaf} remained good (R^2 = 0.47, RMSE = 10.79 μg cm^{-2}; p<0.001). This result was an improvement on the relationship between measured Chl_{Leaf} and a commonly used chlorophyll-sensitive spectral vegetation index; the MERIS Terrestrial Chlorophyll Index (MTCI; R^2 = 0.27, p<0.001). The global maps show large temporal and spatial variability in Chl_{Leaf}, with evergreen broadleaf forests presenting the highest leaf chlorophyll values with global annual median of 54.4 μg cm^{-2}. Distinct seasonal Chl_{Leaf} phenologies are also visible, particularly in deciduous plant forms, associated with budburst and crop growth, and leaf senescence. It is anticipated that this global Chl_{Leaf} product will make an important step towards the explicit consideration of leaf-level biochemistry in terrestrial water, energy and carbon cycle modelling.

Key words: Radiative transfer, 4-Scale, SAIL, PROSPECT, leaf biochemistry, MERIS, satellite, remote sensing, leaf physiology, carbon cycle, ecosystem modelling, phenology

1.0 Introduction

Chlorophyll molecules facilitate the conversion of absorbed solar radiation into stored chemical energy, and the exchange of matter and energy fluxes between the biosphere and the atmosphere. Our ability to accurately model these fluxes is important to forecasting carbon dynamics, within the context of a changing climate. However, within conventional carbon modelling approaches, the parameterisation of vegetation structure and physiological function over both spatial and temporal domains, with an acceptable level of accuracy remains challenging (Groenendijk et al. 2011, Houborg et al. 2015). Within such modelling approaches, leaf area index (LAI) is a core biophysical parameter used to represent vegetation density, seasonal phenology and the fraction of absorbed PAR by vegetation that is converted to biomass (Bonan et al. 2011). The ecological importance of LAI has led to well-validated datasets of LAI maps at global scales and fine spatial resolution (~1 km) (Baret et al. 2013, Deng et al. 2006). However, recent studies have found that a temporal decoupling between vegetation structure and function can occur (Croft, Chen, and Zhang 2014b, Croft, Chen, Froelich, et al. 2015, Walther et al. 2016), particularly in deciduous vegetation with a strong seasonal phenology. Chlorophyll molecules comprise an important part of a plant's "photosynthetic apparatus" (Peng et al. 2011), through the harvesting of light and the production of biochemical energy for use within the Calvin-Benson cycle (Porcar-Castell et al. 2014). Leaf chlorophyll content (Chl_{Leaf}) therefore represents a plant's physiological status, and is closely related to plant photosynthetic function; demonstrating a strong relationship to plant photosynthetic capacity (Vcmax) (Croft et al. 2017). Neglecting to consider chlorophyll phenology within carbon models can lead to an overestimation of the amount of plant carbon uptake at the start and end of a growing season in deciduous vegetation (Croft, Chen, Froelich, et al. 2015, Luo et al. 2018). The incorporation of inter- and intra- annual variations of chlorophyll within ecosystem models has been shown to improve the simulations of carbon and water fluxes (Luo et al. 2018, He et al. 2017).

93 Global efforts to map Chl_{Leaf} have been hampered by the complexity in the relationship between
94 satellite-derived canopy reflectance and plant biophysical and biochemical variables. Thus far, satellite
95 remote sensing applications to map Chl_{Leaf} have largely been limited to empirical methods, via the
96 derivation of statistical relationships between spectral vegetation indices (VIs) and leaf or canopy
97 chlorophyll content (Le Maire, François, and Dufrêne 2004, Sims and Gamon 2002). Indices that include
98 'red-edge' wavelengths (690–740 nm) are the most strongly related to Chl_{Leaf} (Croft, Chen, and Zhang
99 2014a, Malenovský et al. 2013), due to the ready saturation of chlorophyll absorption bands when Chl_{Leaf}
100 exceeds ~30 µg cm^{-2} (Croft and Chen 2018). Some studies have shown promising results using empirical
101 methods (Datt 1998, Haboudane et al. 2002). However, this is usually achieved at local scales, within
102 closely related species (Blackburn 1998) or for uniform, closed canopies, where the vegetation stand
103 essentially behaves as a 'big leaf' (Gamon et al. 2010), and where contributions from other variables,
104 such as background vegetation and non-photosynthetic elements are low. At the leaf level, variations in
105 internal leaf structure, leaf thickness and water content, differentially affect leaf reflectance (Serrano
106 2008, Croft, Chen, and Zhang 2014a). At the canopy scale, vegetation architecture including LAI, foliage
107 clumping, stand density, non photosynthetic elements and understory vegetation, in addition to the
108 sun-view geometry, affect measured reflectance factors (Demarez and Gastellu-Etchegorry 2000,
109 Verrelst et al. 2010, Malenovský et al. 2008).
110
111 An alternative satellite-based approach for deriving Chl_{Leaf} from top-of-canopy reflectance data is
112 through the use of physically-based radiative transfer models. Radiative transfer models provide a direct
113 physical relationship between canopy reflectance and Chl_{Leaf} because they are underpinned by physical
114 laws that determine the interaction between solar radiation and the vegetation canopy. Leaf-level
115 estimation of foliar chlorophyll is achieved by coupling a canopy model and leaf optical model, in a two-
116 step process (Croft and Chen 2018): firstly to derive leaf level reflectance from canopy reflectance and

117 then to derive leaf pigment content from the modeled leaf reflectance (Zhang et al. 2008, Croft et al.
118 2013, Zarco-Tejada et al. 2004). A number of canopy models have been used for this purpose, ranging
119 from turbid medium models (e.g. SAIL) (Verhoef 1984), hybrid geometric optical and radiative transfer
120 models (e.g. 4-SCALE (Chen and Leblanc 1997), GeoSAIL (Huemmrich 2001), DART (Gastellu-Etchegorry,
121 Martin, and Gascon 2004)) in which the turbid media are constrained into a geometric form (i.e. a leaf,
122 shoot, branch and/or crown), and ray-tracing techniques (FLIGHT) (North 1996). At the leaf level, the
123 most widely used leaf optical model is PROSPECT (Jacquemoud and Baret 1990), which has been
124 extensively applied and validated across a wide range of plant species (Malenovský et al. 2006), due to
125 the small number of input parameters required and its ease of inversion. Previous research has
126 demonstrated the strength of this physically-based method for a number of different ecosystems (Zarco-
127 Tejada et al. 2004, Zhang et al. 2008, Croft et al. 2013, Demarez and Gastellu-Etchegorry 2000, Houborg
128 and Boegh 2008). However, this approach has yet to be applied at the global scale.
129
130 This paper presents the first global Chl_{Leaf} map from satellite data using physically-based radiative
131 transfer models. Chl_{Leaf} is defined on a leaf-area basis, as chlorophyll content per half the total surface
132 leaf area. Expressing Chl_{Leaf} by leaf area (as opposed to by dry mass) is the closer representation of what
133 is directly measured by a satellite instrument, and is most appropriate for linking Chl_{Leaf} to ecosystem
134 processes, such as carbon and water fluxes in relation to surfaces (Wright et al. 2004). Chl_{Leaf} is modelled
135 from ENVISAT MEdium Resolution Imaging Spectrometer (MERIS) 300 m reflectance data in a two-step
136 modelling approach, using coupled canopy and leaf radiative transfer models. Modelled Chl_{Leaf} results
137 were subsequently validated using measured ground data at a range of different field sites over six
138 different plant functional types (PFTs). Chl_{Leaf} maps are produced at the global scale every seven days for
139 an entire calendar year 2011 in order to provide spatially- and temporally-distributed leaf chlorophyll
140 content, and consequent physiological information for ecosystem modelling and ecological applications.

2.0 Methods

2.1 Ground data and validation sites

We used measured leaf chlorophyll data from 248 sampling measurements within 28 field locations covering six PFTs (Figure 1 and Table 1) to validate the Chl_{Leaf} retrieval algorithm. These data included 49 measurements in deciduous broadleaf forests (DBF), 9 measurements in evergreen broadleaf forests (EBF), 100 measurements in needleleaf forests (ENF), 55 measurements in croplands (CRP), 28 measurements in grassland (GRS) and 7 measurements in shrublands (SHR).

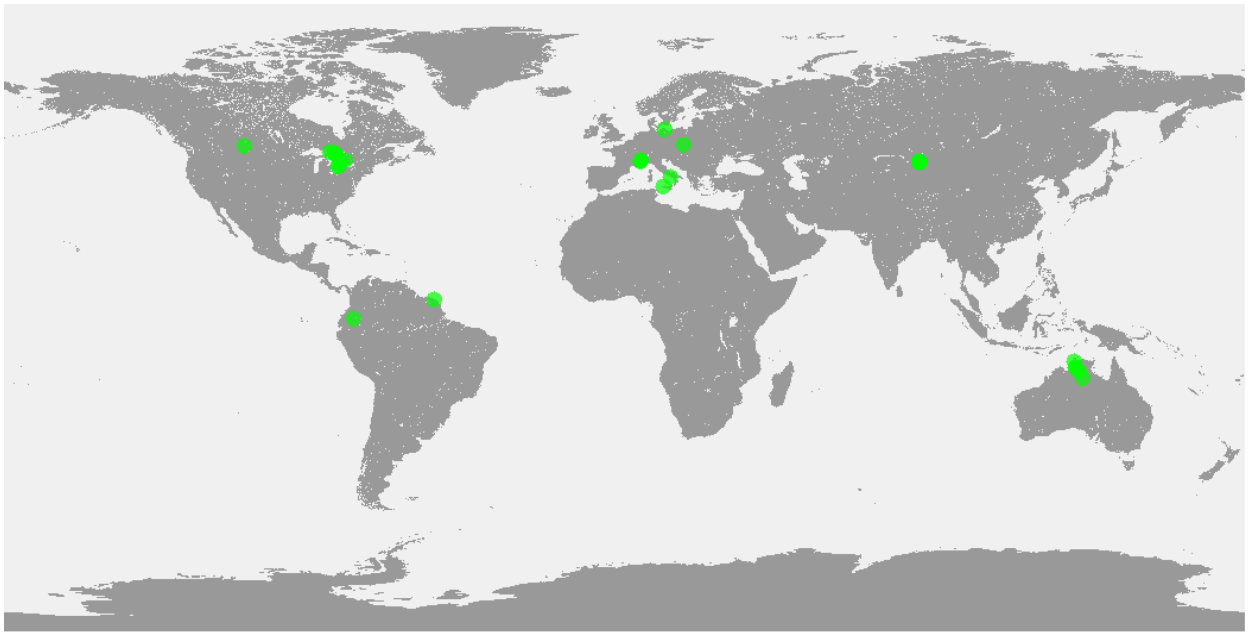

Figure 1: Locations of the twenty-eight field locations used for leaf chlorophyll content validation.

For each field location, the number of discrete sites or dates over which individual ground measurements were taken are reported in Table 1. The number of replicates and spatial sampling varied between the field sites, due to the nature of data collection in individual projects and between researchers, and represents the large number of sources that have come together to produce this work.

156

157 *Table 1: Details of the ground measurements of leaf chlorophyll content used for validation used in this*
158 *study, including the sampling location (Lat = latitude, Long = longitude) and sampling year, dominant*
159 *species, plant functional type (PFT), mean site leaf area index (LAI) value and chlorophyll determination*
160 *method (Chl. method).*

Site name	Country	Sampling years	Lat/ Long*	PFT	Dominant species	Mean LAI	Mean Chl. (μg cm^{-2})	No. of sites/ dates	Chl. method†	Reference
Haliburton	Canada	2004	45.24 -78.54	DBF	Sugar maple	5.5	38.3	8	Lab	Zhang et al. (2007)
Borden Forest	Canada	2013-15	44.32 -79.93	DBF	Red maple	4.2	37.8	13	Lab	Croft et al. (2015)
Bioindicators DBF	Canada	2002	46.84, -81.41	DBF	White birch, poplar	-	34.3	26	Lab	-
Sudbury DBF	Canada	2007	47.16, -81.71	DBF	Trembling aspen	4.3	48.8	2	Lab	Simic et al. (2011)
Amazon FG	French Guyana	2007-08	5.28, -52.92	EBF	-	6.7	62.1	3	Chl. meter	Rowland et al. (2014)
Amazon Ecuador	Ecuador	2012	-0.18, -76.36	EBF	-	-	53.6	6	Field spec.	Arellano et al. (2017)
Sudbury ENF	Canada	2007	47.18, -81.74	ENF	Black spruce		29.0	10	Lab	Simic et al. (2011)
Chapleau	Canada	2012	47.58, -83.01	ENF	Jack pine	3.3	49.3	8	Lab	Croft et al. (2014)
Bioindicators ENF	Canada	2001-02	47.11, -81.82	ENF	Black spruce, Jack pine	-	32.8	60	Lab	-
Sudbury Zhang	Canada	2003-04	47.16, -81.74	ENF	Black spruce	3.2	30.4	18	Lab	Zhang et al. (2008)
Le Casset	France	2008	44.98, 6.48	ENF	European larch	-	60.8	2	Lab	Homolová et al., (2013)
Bily Kriz	Czech Republic	2004, 2006	49.50, 18.54	ENF	Norway spruce	8.2	39.8	2	Lab	Homolová et al. (2013); Malenovský et al. (2013)
Col du Lautaret Terrasses	France	2008	45.04, 6.35	GRS	Mixed alpine sp.	-	38.5	3	Lab	Homolová et al. (2014)
Roche Noir	France	2008	45.06, 6.38	GRS	Mixed alpine sp.	-	39.3	5	Lab	Pottier et al. (2014)
GRS National Park	Canada	2012-14	49.16, -107.56	GRS	Mixed-grass prairie	1.0	35.4	20	Lab	Tong and He (2017)
Stratford Wheat	Canada	2013	43.45, -80.86	CRP	Wheat	2.2	38.7	5	Lab	Dong et al. (2017)

Stratford Corn	Canada	2013	43.46, -80.81	CRP	Maize	2.7	42.4	10	Lab	Dong et al. (2017)
Mosuowanzhen	China	2011	44.19, 85.49	CRP	Cotton	1.87	64.3	15	Lab	Yi et al., (2014)
Sele River Plain	Italy	2009	40.52, 15.00	CRP	Maize, fruit trees	2.3	42.6	29	Chl. Meter •	Vuolo et al. (2012)
Demmin	Germany	2006	53.99, 13.27	CRP	Maize, wheat, Sugarbeet	-	35.4	4	Chl meter	Hajnsek et al. (2006)
Trapani	Sicily	2010	37.64, 12.85	CRP	Olive trees	1.5	39.6	3	Chl. meter	-
Howard Springs	Australia	2009	-12.49, 131.15	SHR	Eucalyptus	1.3	57.7	1	Lab	Amiri (2013)
Daly Uncleared	Australia	2009	-14.16, 131.39	SHR	Eucalyptus	0.8	50.1	1	Lab	Amiri (2013)
Daly Regrowth	Australia	2009	-14.13, 131.38	SHR	Eucalyptus	0.9	45.1	1	Lab	Amiri (2013)
Adelaide River	Australia	2009	-13.08, 131.12	SHR	Eucalyptus	0.7	61.5	1	Lab	Amiri (2013)
Dry Creek	Australia	2009	-15.26, 132.37	SHR	Eucalyptus	0.8	45.9	1	Lab	Amiri (2013)
Sturt Plains Shrubland	Australia	2009	-17.15, 133.35	SHR	Eucalyptus	0.0	58.2	1	Lab	Amiri (2013)
Sturt Plains Woodland	Australia	2009	-17.18, 133.35	SHR	Acacia	0.7	45.1	1	Lab	Amiri (2013)

** where multiple sampling sites are present at a given field location, approximate central co-ordinates are given. DBF = Deciduous broadleaf, ENF = Evergreen needleleaf, EBF = Evergreen broadleaf, GRS = Grassland, CRP = Cropland, SHR = Shrubland. †Lab = laboratory extraction; Chl meter = handheld optical meter; Field spec = field spectrometer. • indicates species specific chl. meter calibration equations.*

Methods of chlorophyll measurement presented in Table 1 were either through laboratory analysis techniques (Lab) or via optical methods (Croft and Chen 2018), i.e. a handheld chlorophyll meter (Chl. meter) or a field spectroradiometer (Field spec.). Where species specific calibration equations were used, further details of the calibration equations can be found in the corresponding referenced paper. The field spectrometer-based retrieval (Arrellano et al., 2017) used the PROSPECT radiative transfer model (Jacquemoud et al., 1990) to estimate chlorophyll content. It is recognised that the different

172 methods of chlorophyll determination may lead to a certain degree of variability between validation
173 measurements. The algorithm was validated according to the closest available ENVISAT MERIS satellite
174 date and location to the field sampling date. Due to the relative scarcity of available *in situ* Chl_{Leaf} data,
175 the existing validation data were maximised by using data collected in years shortly preceding or
176 following the MERIS operational time frame (i.e. earlier than 2002 or later than 2011; Table 1). In this
177 case, the correct day of year (DOY) from the closest calendar year within the 2002-2011 time period,
178 was used. The validation results (Section 3) are partitioned to indicate whether the results are from the
179 current year or closest matched year.
180
181 **2.2 Satellite data**
182 **2.2.1 MEdium Resolution Imaging Spectrometer (MERIS) satellite data**
183 ENIVSAT MERIS satellite-derived reflectance data was selected as the input remote sensing product for
184 this study, due to the sampling of chlorophyll-sensitive red-edge bands, a short temporal revisit time
185 (every 2-3 days) for global application, medium spatial resolution (300 m) and its high radiometric
186 accuracy (Curran and Steele 2005). We used the full resolution (FR) surface reflectance (SR) product,
187 which is produced as a 7-day temporal synthesis from data collected at the original 2-3 day revisit
188 frequency. The global SR time series are produced by a series of pre-processing steps within the MERIS
189 pre-processing chain, including radiometric, geometric, bidirectional reflectance distribution function
190 (BRDF), pixel identification, and atmospheric correction with aerosol retrieval. The 7-day product
191 normalises reflectance to nadir view, and the solar zenith angle is that of 10h00 local time for the
192 median day of the compositing period. MERIS reflectance data is provided in 13 bands (spectral
193 resolution = ~10 nm) in the visible, red-edge and near infra-red bands, with the atmospheric bands
194 (bands 11 and 15) removed. The MERIS FR surface reflectance global time-series covers the 2003-2012
195 time period.

196

197 **2.2.2 Landcover map**

198 A global land cover map produced from 300 m spatial resolution MERIS data, as part of the European
199 Space Agency Climate Change Initiative (CCI-LC) project, from the 5-year period (2008-2012) was used to
200 define PFTs. The legend is based on the UN Land Cover Classification System (LCCS) with the view to be
201 compatible with the Global Landcover 2000 (GLC2000), GlobCover 2005 and 2009 products.

202

203 **2.2.3 Leaf area index (LAI)**

204 Copernicus Global Land Service GEOV1 LAI product derived from SPOT-VGT satellite (Baret et al., 2013)
205 was used in the algorithm, with a global LAI coverage from 1999 to the present at 10-day temporal
206 intervals and a spatial resolution of 1 km. The GEOV1 LAI product is derived from the CYCLOPES v3.1 and
207 MODIS c5 biophysical products, through a neural-network machine-learning algorithm (Baret et al.
208 2013). The selection of CYCLOPES v3.1 and MODIS c5 products takes advantage of previous
209 development efforts and capitalises on the performances of each product (Camacho et al. 2013). As part
210 of the processing chain, the LAI product is reprojected onto the Plate-Carrée 1/112° grid, temporally
211 smoothed, interpolated at the 10-day frequency, and re-scaled to fit the expected range of variation
212 (Verger et al. 2015). GEOV1 LAI products consider clumping as a weighted contribution of CYCLOPES and
213 MODIS products, where MODIS LAI accounts for clumping at plant and canopy scales (Knyazikhin et al.
214 1998), with the exception of needleleaf forests, for which shoot clumping is not accounted for. In the
215 CYCLOPES algorithm, landscape clumping is represented by considering fractions of mixed pixels (Baret
216 et al. 2013). Recent validation studies indicated that GEOV1 outperformed most existing products in
217 both accuracy and precision (Camacho et al. 2013). Validation results showed good spatial and temporal
218 consistency and accuracy, smooth and stable temporal profiles, good dynamic range with reliable
219 magnitudes for bare areas and dense forests (Camacho et al. 2013). The GEOV1 LAI product was

220 selected for this project, because it met the following criteria: a high temporal frequency (every 10
221 days), acceptable spatial resolution (1 km), a long archive of data covering the complete MERIS mission
222 (2002-2012), and strong product validation.
223
224 **2.3 Algorithm development**
225 To derive leaf chlorophyll content from remote sensing data at the global scale, a two-step modelling
226 approach was selected. The first step in the algorithm is the modelling of leaf-level reflectance spectra
227 from satellite-derived canopy reflectance data, using physically-based radiative transfer models to
228 account for the influence of canopy architecture, image acquisition conditions and background
229 vegetation on canopy reflectance. The second step was to retrieve leaf chlorophyll content from the
230 modelled leaf reflectance derived in Step 1, using a leaf optical model. A two-step inversion method is
231 favoured over a coupled one-step inversion because the output of each stage can be assessed
232 individually, and may be validated against measured leaf-level reflectance data at field sites (Croft et al.
233 2013, Zhang et al. 2008). This physically-based canopy inversion method has been previously
234 successfully demonstrated using different combinations of canopy and leaf models (Croft et al. 2013,
235 Moorthy, Miller, and Noland 2008, Zarco-Tejada et al. 2004, Kempeneers et al. 2008).
236
237 For the first step, two canopy reflectance models were selected, according to the structural
238 characteristics of the vegetation present. For spatially heterogeneous 'clumped' vegetation types (i.e.
239 deciduous and coniferous trees, shrubs), the 4-Scale geometrical–optical model (Chen and Leblanc
240 1997) was used (see Section 2.3.1). For homogenous canopies that can be treated as one-dimensional
241 (1D) turbid media, such as agricultural crops, we used the SAIL model (Verhoef 1984) (Section 2.3.2). To
242 invert the canopy radiative transfer models, individual LUTs for different PFTs were created, based on
243 variable and fixed input parameters (Table 2 and Table 3). The LUT approach was selected to optimise

computational resources and reduce problems associated with appearances of local minima, given sufficient sampling of the variable space (Jacquemoud et al. 2009). Whilst these structural parameterisations are important, their influence on canopy reflectance is mediated by LAI, which is the dominant driver of modelled canopy reflectance (Zhang et al. 2008 and Section 2.4). The availability of accurate and well validated global-scale LAI products facilitated the treatment of LAI as a variable parameter, which was derived from the GEOV1 LAI product (Section 2.2.3) at 10 day intervals and 1 km spatial resolution. In the second step, leaf chlorophyll content was retrieved using a leaf optical model (PROSPECT; Jacquemoud and Baret 1990) (Section 2.3.3) from the modelled leaf reflectance that was derived in step 1.

2.3.1 Step 1: Leaf reflectance inversion - 4-Scale model

The 4-Scale model (Chen and Leblanc 1997) was selected for the inversion of leaf level reflectance from satellite-derived images in forested and spatially clumped ecosystems. 4-Scale considers the three-dimensional (3D) spatial distribution of vegetation groups and vegetation crown geometry, in addition to the structural effects of branches and scattering elements. In closed canopies, structural variables such as crown shape and clumping of foliage elements are dominant, whereas in open canopies the effects of background reflectance and shadows prevail. The 4-Scale model simulates the Bidirectional Reflectance Distribution Function (BRDF) based on canopy architecture described at four scales: 1) vegetation grouping, 2) crown geometry, 3) branches, and 4) foliage elements (Chen and Leblanc 2001). A crown is, therefore, represented as a complex medium, where mutual scattering occurs between shoots or leaves. Consequently, sunlit foliage can be viewed on the shaded side and shadowed foliage on the sunlit side. Reflected radiance from different scene components is calculated by first separating sunlit and shaded components through first-order scattering, and then adding multiple scattering from subsequent interactions with vegetation elements or background material (Chen and Leblanc 2001). To

model canopy reflectance, the 4-Scale model was run in the forward mode, with variable (LAI, solar zenith angle and view zenith angle) and fixed structural parameters and background reflectance spectra (Table 2), set according to ground measurements and values reported in the literature (Chen and Leblanc 1997, Leblanc et al. 1999). The element clumping index (ΩE) represents vegetation clumping at scales larger than the shoot, and is associated with canopy architecture and structural variables, such as crown size and vegetation density. ΩE is an important parameter for estimating radiation interception and distribution in plant canopies (Chen, Menges, and Leblanc 2005). The non-random spatial distribution of trees is simulated using the Neyman type A distribution to permit clumping and patchiness within a forest stand (Chen and Leblanc 1997).

Table 2: Fixed and variable parameters used in the 4-Scale model for LUT generation. Broadleaf/needleleaf classes include respective deciduous and evergreen plant functional types.

	Broadleaf trees	Needleleaf trees	Shrubland	References
LAI (m^2 m^{-2})	0.1-8	0.1-8	0.1-8	Baret et al., (2013)
Solar zenith angle (°)	20-70	20-70	20-70	MERIS metadata
View zenith angle (°)	0	0	0	MERIS metadata
Relative azimuth angle (°)	0	0	0	MERIS metadata
Stick height (m)	10	10	3	Los et al. (2012)
Crown height (m)	8	10	7	Los et al. (2012)
Crown shape	Spheroid	Cone & cylinder	Spheroid	Chen and Leblanc (1997)
Tree density (trees/ha)	1400	3000	1000	Chen et al. (1997) & Leblanc et al. (1999)
Crown radius (m)	1.25	1.0	1.25	Chopping et al. (2008), Evans et al. (2015) & Thorpe et al. (2010)
Neyman grouping	3	4	3	Leblanc et al. (1999)
Clumping index (ΩE)	0.90	0.80	0.80	Pisek et al. (2011)
Needle to shoot ratio (γE)	1	1.4	1	Pisek et al. (2011)
Foliage element width (m)	0.15	0.1	0.15	Chen and Cihlar (1995) & Leblanc et al. (1999)
Background composition	Green vegetation and soil	Green vegetation and soil	Dry grasses and soil	Observations/ measurements

According to the specified input parameters, the 4-Scale model calculates canopy reflectance (ρ) as a linear summation of four components:

$$\rho = \rho_{PT\lambda} F_{PT} + \rho_{ZT\lambda} F_{ZT} + \rho_{PG\lambda} F_{PG} + \rho_{ZG\lambda} F_{ZG} \quad \text{[Eq. 1]}$$

where the reflectance factors from each scene component are: sunlit vegetation ($\rho_{PT\lambda}$), shaded vegetation ($\rho_{ZT\lambda}$), sunlit ground ($\rho_{PG\lambda}$) and shaded ground ($\rho_{ZG\lambda}$), and F_{PT}, F_{PG}, F_{PG} and F_{ZT} represent the probability of viewing each component, respectively (Chen and Leblanc 2001). The 4-Scale model

includes a multiple scattering scheme, for 2nd order scattering and above, through computing the interactions among the four scene components based on view factors from one component to the other (Chen and LeBlanc, 2001). In this unique way, the geometrical effects propagate to all orders of multiple scattering. In order to derive leaf reflectance ($\rho_{L\lambda}$) from sunlit crown reflectance (ρ_{PT}), the enhancement of both sunlit and shaded reflectance due to multiple scattering is accounted for using a multiple scattering factor (Zhang et al. 2008, M factor; Croft et al. 2013, Simic, Chen, and Noland 2011). The M factor can be calculated using the output sunlit and shaded scene components from 4-Scale:

$$M_\lambda = \frac{\rho_\lambda - \rho_{PG\lambda} F_{PG}}{\rho_{L\lambda} F_{PT}} \quad \text{[Eq. 2]}$$

Finally, the M factor (Eq. 2) is used to derive leaf reflectance from canopy-level satellite reflectance ($\rho_{satellite}$), by converting sunlit crown reflectance into sunlit leaf reflectance, and allowing the inclusion of the less variable shaded components (Eq. 3).

$$\rho_{L\lambda} = \frac{\rho_{satellite\lambda} - \rho_{PG\lambda} F_{PG}}{M_\lambda F_{PT}} \quad \text{[Eq. 3]}$$

2.3.2 Step 1: Leaf reflectance inversion - SAIL model

The SAIL radiative transfer model (Verhoef 1984) was used to derive leaf reflectance from satellite-derived images in cropland and grassland ecosystems, where the distribution of foliage approaches randomness, and information on canopy structural variables such as crown shape and the clumping of foliage elements is not applicable. Turbid medium models such as SAIL (Verhoef, 1984) assume that the canopy is composed of homogeneous, horizontal layers of Lambertian scatterers randomly distributed in

space. The SAIL model is one of the most popular and well validated models used in agricultural systems (Jacquemoud et al. 2009, Darvishzadeh et al. 2008, Clevers and Kooistra 2012). SAIL is based on Suit's model (Suits 1971), which is founded on a set of four differential equations: (1) diffuse incoming flux, (2) diffuse outgoing flux, (3) direct solar flux, and (4) flux with radiance in the direction of remote sensing observation. Table 3 details the fixed and variable parameters used within the SAIL model, based on field observations and literature (Privette et al. 1996, Darvishzadeh et al. 2008) that were used to model canopy reflectance for the LUT-based inversion.

Table 3: Fixed and variable parameters used in the SAIL model for LUT generation.

	Cropland	**Grassland**	**References**
Leaf area index	0.1 - 8	0.1 - 8	Baret et al., (2013)
Solar zenith angle (°)	20-70	20-70	MERIS metadata
View zenith angle (°)	0	0	MERIS metadata
Relative azimuth angle (°)	0	0	MERIS metadata
Leaf inclination distribution function	Ellipsoidal	Erectophile	Clevers and Kooistra (2012) & Zou and Mõttus (2015)
Hot spot parameter (m m^{-1})	0.1	0.1	Darvishzadeh et al. (2008) & Vohland and Jarmer (2008)
Soil factor (dimensionless)	1	0.4	Observations/ measurements

The leaf inclination distribution function (LIDF) describes the frequency distribution of leaf inclination angles in different directions. For agricultural crops, LIDF is ellipsoidal (Campbell, 1986), with the mean leaf inclination angle set at 40°, in line with values measured within previous studies (Zou and Mõttus 2015, Liu, Pattey, and Jégo 2012). For grasslands the LIDF is erectophile (LiDFa = -1, LiDFb = 0) (Clevers and Kooistra 2012, Sandmeier et al. 1999, He, Guo, and Wilmshurst 2007, Verma et al. 2017, Migliavacca et al. 2017). The hot spot (Hs) parameter is defined as the ratio between the average leaf size and the height of the canopy (Darvishzadeh et al. 2008, Verhoef 1985). The soil factor (Sf) accounts for

variations in the brightness of the soil background, where a value of 0 denotes a wet soil and 1 a dry soil. A LUT was generated from the fixed and variable parameters shown in Table 3, which contains the ratio of the modelled canopy reflectance from the SAIL model to the SAIL input leaf reflectance as a scaling factor (S Factor$_\lambda$). Modelled leaf reflectance ($\rho_{L\lambda}$) is retrieved from satellite canopy reflectance ($\rho_{Satellite\lambda}$) according to Equation 4.

$$\rho_{L\,\lambda} = \rho_{Satellite\,\lambda} * S\,Factor_\lambda \quad \text{[Eq. 4]}$$

2.3.3 Step 2: Deriving leaf chlorophyll content – PROSPECT model

The leaf radiative transfer model PROSPECT (Jacquemoud and Baret 1990, Feret et al. 2008) is used to derive Chl_{Leaf} from the modelled leaf reflectance spectra generated in step one (Section 2.3.1 and 2.3.2). In PROSPECT-5, leaf reflectance and transmittance (400-2500 nm) are defined as a function of six parameters: structure parameter (N), chlorophyll (a+b) concentration (C_{ab}), carotenoid content (Car), brown pigment (C_b), dry matter (C_m) and equivalent water thickness (C_w). Absorption is calculated as the linear summation of the specific absorption coefficients of the biochemical constituents and their respective concentrations. PROSPECT has had widespread validation across a large number of vegetation species and plant functional types (Croft, Chen, Zhang, et al. 2015, Demarez and Gastellu-Etchegorry 2000, Darvishzadeh et al. 2008, Malenovský et al. 2006). Whilst previous studies inverted PROSPECT by iteratively minimising a merit function (Croft et al., 2013), the large volume of data used in this study precluded this option. In order to optimise computational resources, using a vegetation index (VI) based inversion approach. PROSPECT was run in the forward mode to derive chlorophyll-sensitive spectral vegetation indices, according to incrementing chlorophyll content values. The leaf biophysical parameters were varied for each PFT (Table 4), based on measured values and within reported ranges in the literature.

Table 4: Leaf parameters used in the PROSPECT model, along with the vegetation index (VI) derived from forward-modelled reflectance spectra for each plant functional type. C_{ab} = chlorophyll content; N = structural parameter; Car = carotenoid content; C_b = brown matter; C_m = dry matter content; C_w = equivalent water thickness.

	C_{ab} (µg cm^{-2})	N (unitless)	Car (µg cm^{-2})	C_b	C_m (g cm^{-2})	C_w (g cm^{-2})	Vegetation index	Reference
DBF	0-100	1.2	Chl/7	0	0.005	0.01	$MERIS_{SR}$	Féret et al. (2011)
EBF	0-100	1.8	Chl/7	0	0.005	0.01	$MERIS_{SR}$	Arellano et al. (2017)
DNF	0-100	2.8	Chl/7	0	0.05	0.01	$MERIS_{ND}$	De Santis et al. (2009) & Kötz et al. (2004)
ENF	0-100	2.8	Chl/7	0	0.05	0.01	$MERIS_{ND}$	De Santis et al. (2009) & Kötz et al. (2004)
SHR	0-100	1.8	Chl/7	0	0.005	0.01	$MERIS_{ND}$	Enrique et al. (2016) & Sow et al. (2013)
CRP	0-100	1.4	Chl/7	0	0.015	0.01	$MERIS_{ND}$	Jacquemoud et al. (2000)
GRS	0-100	1.2	Chl/7	0	0.005	0.01	$MERIS_{ND}$	Darvishzadeh et al. (2008)

The VIs used in the VI-based PROSPECT inversion are focussed on the red-edge reflectance bands that are resistant to saturation at high chlorophyll values. Croft et al., (2014a) found strong relationships between normalised difference (ND) and simple ratio (SR) vegetation indices with chlorophyll content (Zarco-Tejada et al. 2001, Mutanga and Skidmore 2004), which were modified to MERIS red-edge spectral bands as follows:

$$MERIS_{ND} = \frac{R_{754} - R_{709}}{R_{754} + R_{709}} \quad \text{[Eq. 5]}$$

$$MERIS_{SR} = \frac{R_{754}}{R_{709}} \quad \text{[Eq. 6]}$$

where R is reflectance at given wavelength λ in nm ($R\lambda$). Regression equations were then generated between incrementing chlorophyll content and the modelled VI from PROSPECT (Figure 2), which are then applied to the modelled leaf level reflectance derived from canopy model inversion in Step 1 (Sections 2.2.1 and 2.2.2) to derive the final Chl_{Leaf} values.

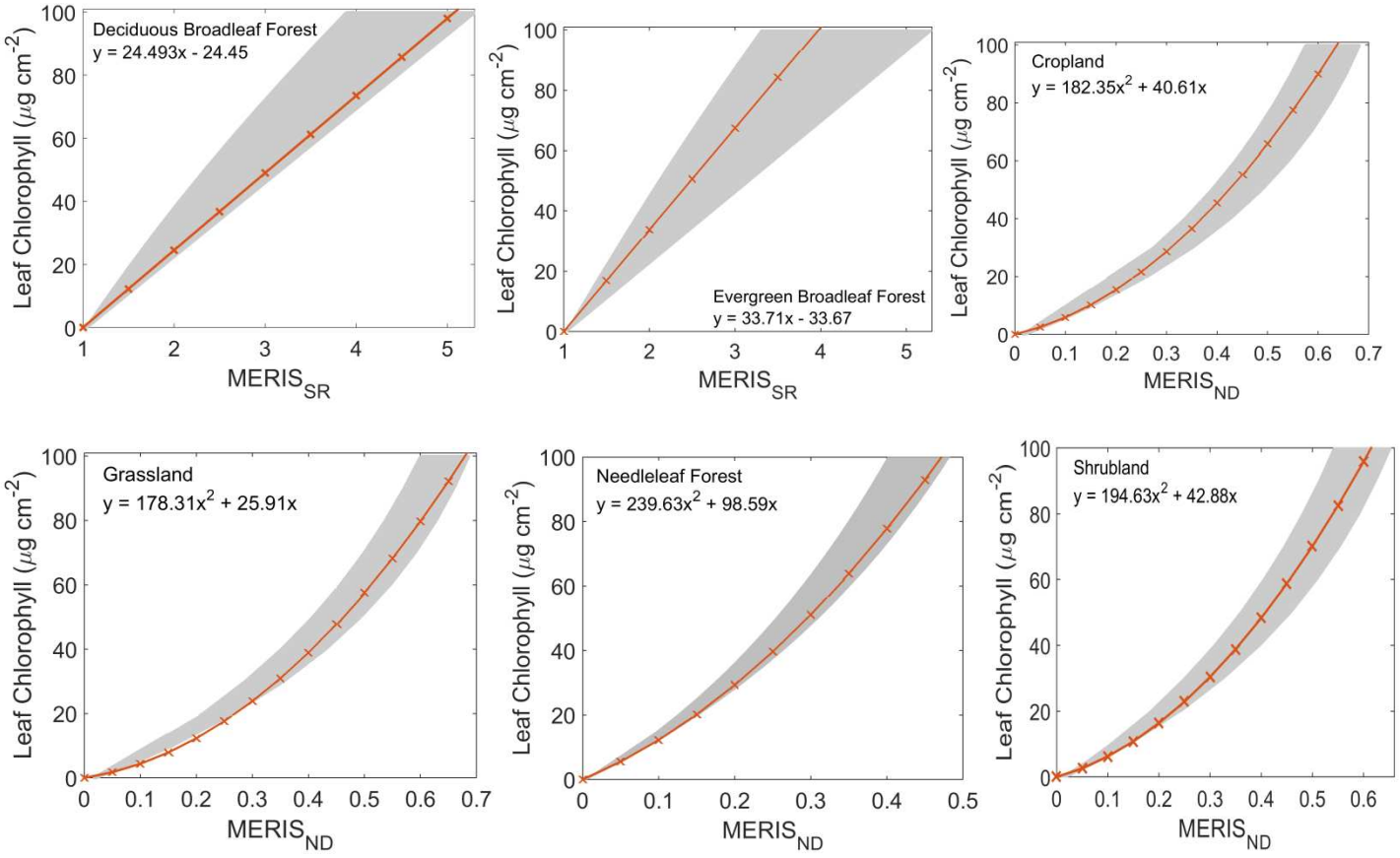

Figure 2: Regression equations for the PROSPECT-based leaf chlorophyll inversion. The shaded grey area represents the potential uncertainty of the forward modelled vegetation index values, according to a range of measured PROSPECT parameter values from published data. For all plant functional types apart from needleleaf forests, the range in input values is two standard deviations either side of the mean from the LOPEX dataset. For needleleaf forests uncertainty values from Kötz et al. (2004) were used.

The shaded grey area in Figure 2 indicates the degree of uncertainty arising from the VI-inversion step, according to the fixed biophysical parameters that are used to parameterise the PROSPECT model. Measured N, C_m and C_w values from the LOPEX published dataset of leaf reflectance and biophysical parameters (Hosgood et al. 1995) were used for DBF, SHR, GRS, CRP species. For the needleleaf and EBF species, for which large measured datasets are not so widely available, we used parameter uncertainty values from Kötz et al. (2004) and standard deviations from Ferreira et al. (2013) for needleleaf and EBF species, respectively. For DBF, SHR, GRS, CRP and EBF species, the PROSPECT model was run in the forward mode for input parameter values that represented two standard deviations of the mean N, C_m and C_w values within the published datasets (represented by grey shading), for each PFT individually. The orange line represents the relationship between the VI and Chl_{Leaf} using the structural parameters in Table 4. The regression equation shown is the empirical model that is used to convert modelled leaf level reflectance derived in Step 1 (Sections 2.3.1 and 2.3.2) to Chl_{Leaf}.

The VI-based PROSPECT inversion method was assessed against the conventional PROSPECT inversion method of iteratively minimising a merit function (Feret et al., 2008), for the ground validation sites detailed in Table 1. The relationship between the modelled Chl_{Leaf} from the VI-inversion and modelled Chl_{Leaf} from the merit function inversion was $R^2 = 0.74$ (percentage bias = 20% and RMSE = 11.01 µg cm^{-2}). Moreover, the VI-inversion increased the relationship between modelled and measured Chl_{Leaf} by 20% ($p<0.001$), when compared to the merit function Chl_{Leaf} inversion. Using VIs centred on the chlorophyll-sensitive red-edge rather than inverting the model across the full leaf spectra reduces the confounding influence of other biophysical variables, such as leaf structure and carotenoid content. Several studies have found a high redundancy of wavelength channels in vegetation studies (Jacquemoud et al., 1995; Simic and Chen, 2008, Croft et al. 2015). Thenkabail et al. (2004) reported that the data volume can be

reduced by 97% when hyperspectral wavebands are reduced to the first five principal components, and still explain close to 95% of data variability. A reduction in spectral data may therefore permit a better model fit over the more sensitive and relevant wavelength ranges.

2.4 Canopy model inversion sensitivity analysis

A sensitivity analysis was undertaken to assess the impact of canopy structural parameters values differing from the fixed value used in the inversion algorithm on the modelled Chl_{Leaf} value. Four of the major PFTs with different structural parameterisations and that employed radiative transfer models (DBF, ENF, CRP, GRS) were tested. All values were held constant according to the values used in the chlorophyll inversion algorithm (Tables 2 and 3), with one parameter incrementally perturbed. The value zero represents the condition under which the structural parameters are consistent with the values used in the main chlorophyll inversion algorithm, as outlined in Tables 1 and 2 (i.e. the reference case). In the case of LAI, which is a variable parameter in the algorithm we used a representative value (LAI = 2.5 (GRS), 4.0 (CRP), 5.0 (ENF), 4.0 (DBF)) as found in a global analysis by Asner et al., (2003), for each PFT to avoid bias from an extreme case. Solar and view zenith angles were held constant at 40° and 0°, respectively. To achieve comparability between structural parameters, results are scaled to a percentage difference from the reference case. The chlorophyll values are shown as an absolute difference from the reference case, in order to provide an estimate of the impact that deviations in the actual structural parameter values from the one used in the modelling algorithm has on modelled leaf chlorophyll content values. The structural parameters vary slightly between the PFTs and two models (PROSAIL and 4-Scale), according to the structural parameters present in the model.

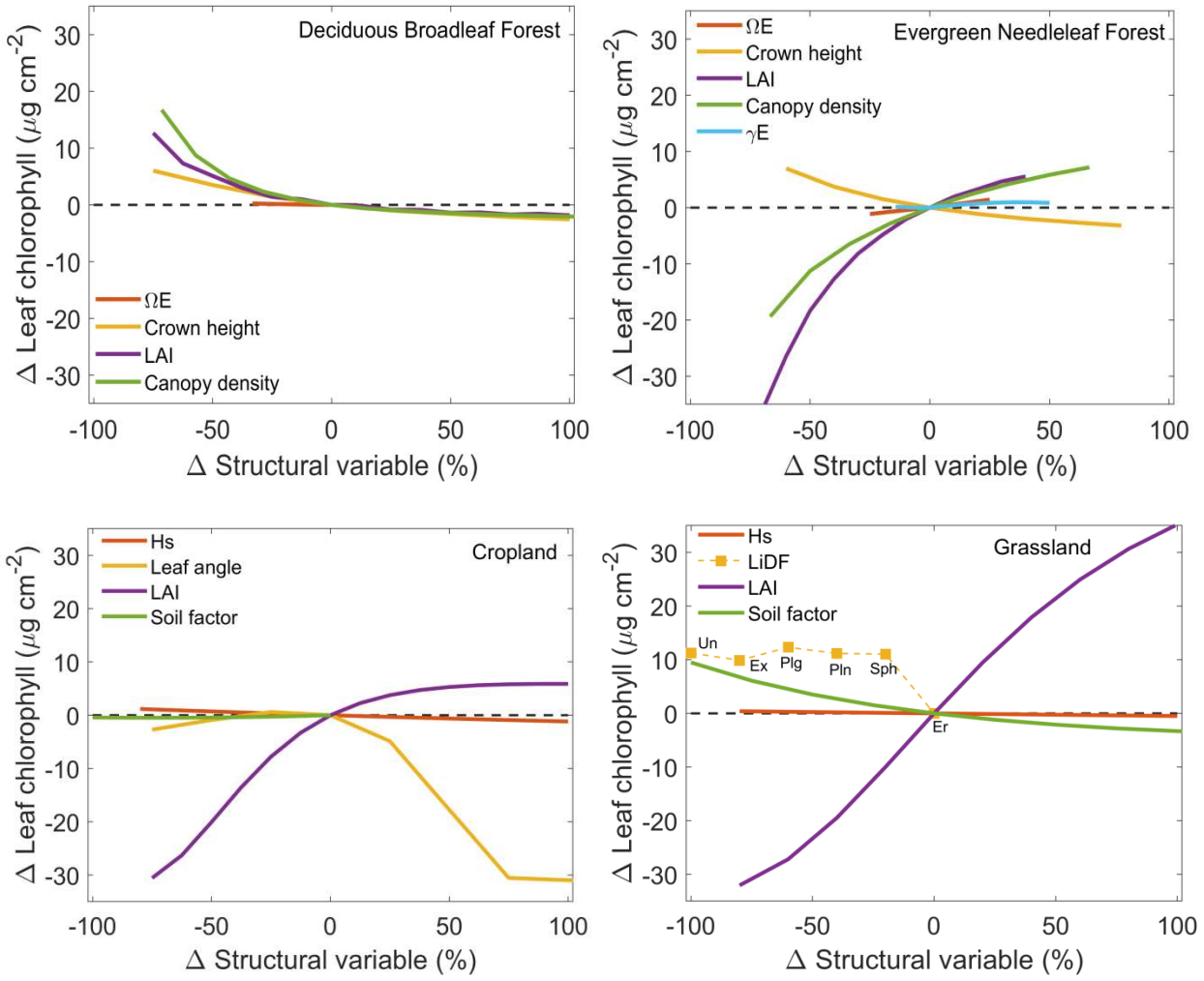

Figure 3: Sensitivity of modelled chlorophyll values to variations in structural parameters within the 4-Scale and SAIL models, for a) deciduous broadleaf forests, b) evergreen needleleaf forests, c) Croplands, d) Grasslands. Zero percentage change (x axis) represents the reference case, where all structural parameters are those used in the algorithm inversion in Table 2 and 3. For grassland results, the different LiDFs are imposed on the x axis scale with LIDF names indicated, where Un = Uniform, Ex = Extremophile, Plg = Plagiophile, Pln = Planophile, Sph = Spherical, Er= Erectophile.

Figure 3 reveals different sensitivities of modelled Chl_{Leaf} values in response to changing a specific structural parameter. In all cases variations in LAI presented a dominant effect on the modelled chlorophyll content. For crops a 25% difference in LAI from the reference case (i.e. LAI = 3.0 and 5.0), resulted in a change in modelled chlorophyll by -7.8 µg cm^{-2} and +3.76 µg cm^{-2}. The asymmetric response of the modelled Chl_{Leaf} values to LAI deviations represents the non-linear response of canopy reflectance to increasing LAI, which saturates at higher LAI values. In the GRS results, this saturation does not occur because of the erectophile leaf inclination angle distribution, and because the LAI reference case is lower (LAI = 2.5), resulting in smaller maximum values (GRS +Δ100% LAI = 5.0, CRP +Δ100% LAI = 8.0). For ENF trees, using the 4-Scale model, variations in canopy density also presented a high degree of sensitivity in modelled Chl_{Leaf} values at extreme low canopy density values. A 33% difference in density from the reference case (i.e. 2000 stems/ha and 4000 stems/ha), resulted in a change in modelled chlorophyll by -6.4 µg cm^{-2} and +4.4 µg cm^{-2}, while a 66% difference resulted in a -19.4 µg cm^{-2} and +7.17 µg cm^{-2} change. For ENF and DBF, deviations in other structural parameters (ΩE, crown height and γE for ENF species) presented a smaller impact on the modelled Chl_{Leaf}. A 20% difference in crown height, for example, only affected Chl_{Leaf} values by +1.5 µg cm^{-2} and -1.18 µg cm^{-2}. For the SAIL model parameters in CRP plants, in addition to LAI, the leaf angle distribution (fixed value = 40°) also strongly affected modelled Chl_{Leaf} at larger leaf inclination angles, approaching more erectophile leaf inclination angles (>60°). From leaf angle distribution = 10° to 50° the imposed variations in modelled chlorophyll were -2.7 µg cm^{-2} to -4.9 µg cm^{-2}. This result was also consistent for the GRS results, where the different LIDFs are noted in Figure 3d. The LIDFs exhibited little change until the leaf inclination angle approached those associated with erectophile canopies, with the plagiophile LIDFs exhibiting the largest difference in chlorophyll values from the modelled erectophile reference case (+12.3 µg cm^{-2}). Changes in the soil factor and the hotspot parameter induced very little differences in modelled Chl_{Leaf}. For example, in CRP plants a +100% change in the hotspot value (Hs = 0.2) only

resulted in a -1.2 μg cm^{-2} in Chl_{Leaf}, confirming the findings of Vohland and Jarmer (2008). Deviations in Chl_{Leaf} values that are close to zero, with increasing percentage change in the structural parameter indicates a greater tolerance of the model algorithm to differences in the actual structural parameter value at a given site, to the value that is fixed in the model. The inclusion of LAI as a variable parameter mitigates against much of the uncertainty generated in incorrect structural parameters, provided the satellite-derived LAI value is reasonable. Underestimations of the actual ground LAI value by the satellite product may therefore cause substantial uncertainty in modelled Chl_{Leaf} results.

2.5 Data smoothing and gap-filling

The Locally Adjusted by Cubic-Spline Capping (LACC) method (Chen, Deng, and Chen 2006) was developed to produce continuous seasonal trajectories of satellite-derived surface parameters contaminated by clouds and other atmospheric effects. The LACC method previously has been used successfully to smooth time series of clumping index and NDVI (He et al. 2016). Contaminated points can be identified in the time series and replaced with expected values through temporal interpolation between adjacent valid points. For identifying atmospherically contaminated points in a time series, a cubic-spline curve fitting technique with a curvature constraint was developed. Without this curvature constraint, the fitted polynomial curve would also fit the contaminated points, defeating the study purpose. In the LACC algorithm, a maximum global curvature of 0.5 is prescribed in the first step to identify contaminated points. In the second step, the curvature is adjusted locally (i.e. at different dates of the year) according to the local shape of the curve fitted with the global curvature constraint. This adjustment is to enhance the large curvatures generally found at the beginning and the end of a growing season, or double cropping seasons, and to reduce the curvature during a non-growing season and/or around the peak of growing seasons. In this way, smooth trajectories that also follow the rapid growing season variation patterns can be produced. In this study, the LACC algorithm is used to identify

contaminated data points and to gap-fill missing data points. However, in tropical areas there are often fewer than the required six data points needed to run the LACC algorithm. In this case, in order to derive temporally continuous data across the year, we removed the highest and lowest data point and linearly interpolated across the year. In northern latitude evergreen needleleaf forests where snow cover prevented acquisition of surface reflectance data from the vegetation canopy, we took the mean seasonal value and extended it across the year. Whilst such temporal gap-filling is likely to introduce some uncertainty in the modelled chlorophyll results, the temporal variations in chlorophyll content for these PFTs is small relative to deciduous forests or croplands. The annual global distribution of leaf chlorophyll content maps that are presented in this paper are for the last full year that MERIS was operational (2011). Missing data due to cloud or MERIS image acquisition limitations (Tum et al. 2016) are gap-filled with corresponding 2010 data from the same DOY within the LACC smoothing algorithm for spatial completeness and visual assessment. The original 2003-2011 global maps are also available for use within the academic community.

3.0 Results and Discussion

The annual global distribution of leaf chlorophyll content is presented in Figure 4a, with the geographic trends varying both within and between biomes. Figure 4b depicts the annual range in chlorophyll values for the major PFTs, as an integration of the temporal and spatial variability in chlorophyll content over a year and across the globe.

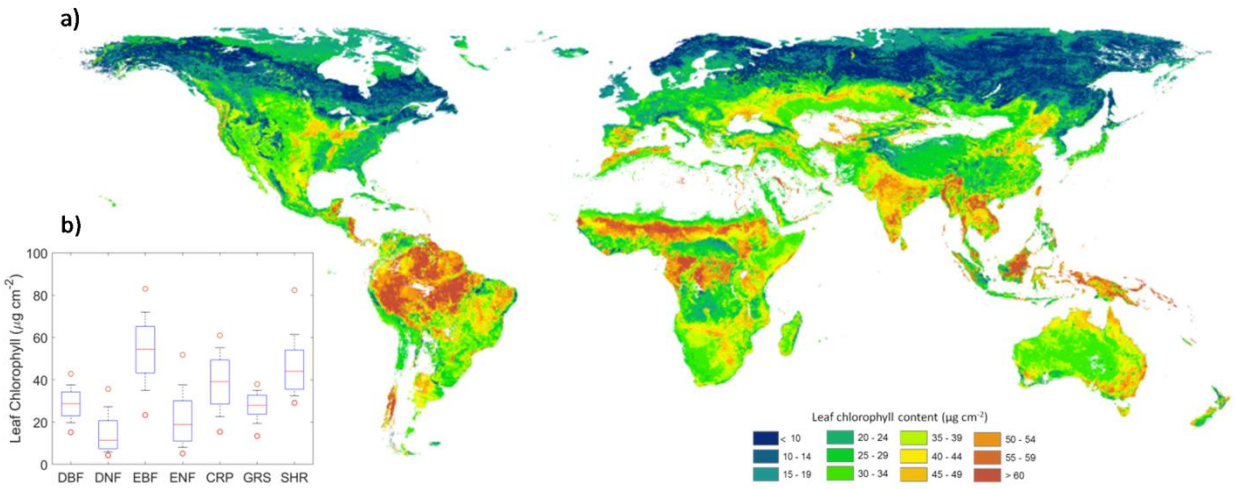

Figure 4: a) The spatial distribution of median annual global distribution of leaf chlorophyll content (at 9 km resolution), and b) the median and interquartile range of leaf chlorophyll content, along with extreme values given for 9% and 91% (whiskers) and 2% and 98% (circles) of the data range.

On an annual basis, the highest median Chl_{Leaf} values are present in evergreen broadleaf forests (54.4 μg cm^{-2}; Figure 4b), which is in part due to the high chlorophyll content of the vegetation present, and also due to the lack of seasonal leaf loss. The lower median annual chlorophyll values (Figure 4b) are consequently found in deciduous biomes (broadleaf and needleleaf forests, 28.8 μg cm^{-2} and 11.4 μg cm^2, respectively). Ground measurements have previously demonstrated that nitrogen-poor needleleaf species typically exhibit lower chlorophyll contents by unit area than broadleaf species (Middleton et al. 1997), which is also evident in the median annual results shown in Figure 4 (ENF, 18.9 μg cm^{-2}). Environmental constraints may also impact Chl_{Leaf} values, through temperature extremes or water availability in evergreen PFTs. Temperate grasslands, for example, are often located in regions that experience extreme annual temperature variability (McGinn 2010), which affects chlorophyll biosynthesis (Ashraf and Harris 2013). From the global map of median annual Chl_{Leaf}, the footprints of

some agricultural regions are also clearly detectable, for example the 'Corn Belt' in Midwestern USA, throughout India, the Loess belt in central Europe and in northeastern China, due to their higher annual peak values, which may be related to fertilization application.

3.1 Validation of modelled leaf chlorophyll estimates for individual PFTs

The leaf chlorophyll algorithm was validated using 248 samples, across a number of different sampling dates and years. The modelled chlorophyll results are plotted against ground-measured values for all available PFTs (Figure 5).

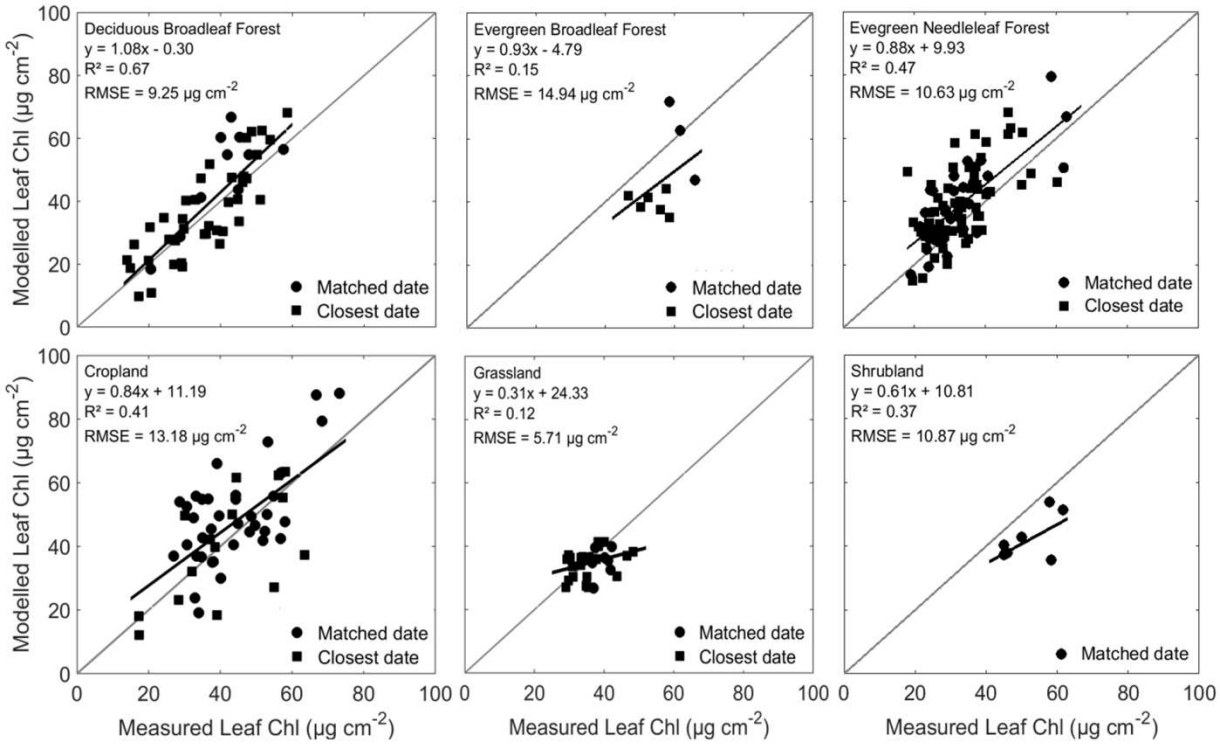

Figure 5: Validation of modelled leaf chlorophyll with measured ground data for individual plant functional types. Data are distinguished between temporally matched sampling and satellite overpass dates, and for ground data collected outside the MERIS lifespan (2002-2012), the closest satellite date was selected.

553

554 The strongest performances are seen for DBF (R^2 = 0.67; RMSE = 9.25 μg cm^{-2}, relative RMSE = 25.4%)
555 followed by ENF (R^2 = 0.47; RMSE = 10.63 μg cm^{-2}, relative RMSE = 32.62%) and CRP (R^2 = 0.41; RMSE =
556 13.18 μg cm^{-2}, relative RMSE = 30.8%). Nonetheless the other three PFTS also showed similar levels of
557 uncertainty, where relative RMSE values were 26.5%, 15.7% and 20.8% for EBF, GRS and SHR,
558 respectively. The statistics reported in Figure 5 are for combined temporally matched sampling and
559 satellite overpass dates, and for ground data collected outside the MERIS lifespan (2002-2012), where
560 the closest satellite date was selected (See Section 2.1). For comparison, the regression results using
561 only the matched dates inside the MERIS operational window are: DBF: R^2 = 0.63, p<0.001; ENF: R^2 =
562 0.63, p<0.001; EBF: insufficient data; and CRP: R^2 = 0.43, p<0.001. The shrub data used in Figure 5 only
563 contained matched dates. The regression results for all dates combined and only matched dates are
564 comparable, with the largest difference arising for EBF, which has fewer data and a smaller dynamic
565 range.

566

567 **3.2 Overall validation and comparison with vegetation indices**

568 The transferability of an algorithm across spatial and temporal scales is essential for modelling Chl_{Leaf}, or
569 any ecological variable, at the global scale. In comparison to empirical approaches (Gitelson, Gritz, and
570 Merzlyak 2003, Roberts, Roth, and Perroy 2016, Peng et al. 2017), the nature of physically-based
571 retrieval methods can account for relationships between canopy reflectance and Chl_{Leaf} across different
572 species and measurement acquisition conditions. Regressions between measured and modelled Chl_{Leaf}
573 for all PFTs combined are shown in Figure 6, alongside results for two popular vegetation indices with
574 the same measured Chl_{Leaf} data (the chlorophyll-sensitive MERIS Terrestrial Chlorophyll Index (MTCI =
575 754 nm-709 nm/709 nm-681 nm) and the Normalised Difference Vegetation Index (NDVI = 865 nm-664
576 nm/865 nm+664nm)).

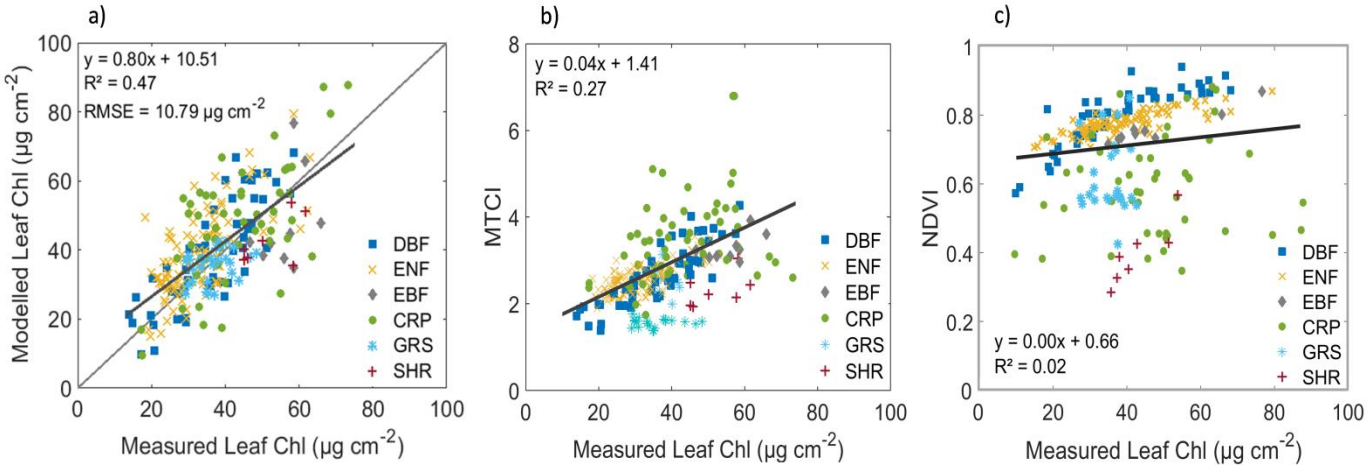

Figure 6: Relationships between measured leaf chlorophyll content and a) physically-based modelled chlorophyll content; b) MERIS Terrestrial Chlorophyll Index (MTCI) values and c) Normalised Difference Vegetation Index (NDVI) values.

Figure 6a demonstrates the suitability of the Chl_{Leaf} algorithm for application across multiple PFTs, with a strong, linear relationship for all PFTs combined (R^2 = 0.47; p<0.001). By contrast, the MTCI regression is weaker (R^2 = 0.27; p<0.001), with some separation in MTCI values according to PFT. Cropland and DBF, for example, exhibit higher values than grassland and shrubland, for the same Chl_{Leaf}. This stratification is likely to due to the strong influence of LAI on MTCI values. Nonetheless, MTCI does present a relative improvement over NDVI results (R^2 = 0.02; n/s), due to the inclusion of chlorophyll-sensitive red-edge bands within the VI. The biomass-sensitive NDVI values also exhibit a separation according to PFT, due to differences in canopy structure and background, with cropland and grasslands also presenting particular variability in values within the same PFT. This result points to the importance of accounting for variations in canopy structure when deriving leaf-level chlorophyll results, and has implications for

applying VIs over large spatial extents to infer information on physiological processes or plant productivity.

3.4 Leaf chlorophyll phenology and temporal trends

The annual variability in leaf chlorophyll content was evaluated through the standard deviation of mean annual Chl_{Leaf}, (Figure 7a). The seasonal phenology of mean Chl_{Leaf} and mean LAI across the northern hemisphere are shown for different biomes in Figure 7b.

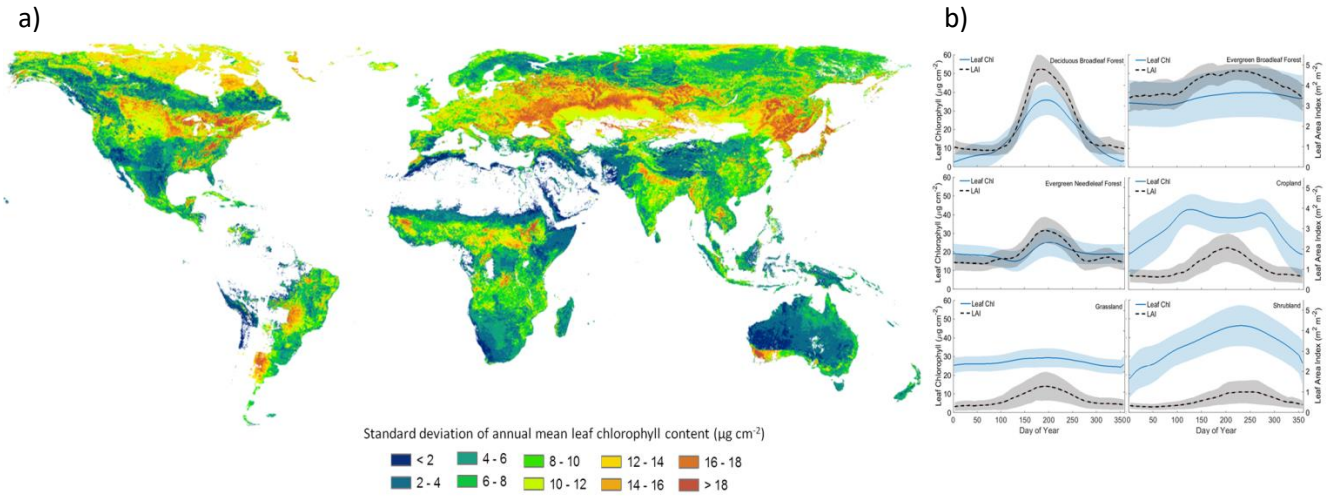

Figure 7: Global 2011 maps of a) seasonal variability in leaf chlorophyll (one standard deviation of one year time series), and b) mean seasonal phenologies of modelled chlorophyll content and LAI across the northern hemisphere for six different plant functional types during 2011. Shaded area indicates one standard deviation.

Global regions that contain large areas of deciduous forests and croplands, which are dominated by a strong seasonal phenology, present the largest temporal variation and dynamic range in Chl_{Leaf} values (Figure 7a). In Figure 7b, DBF displays an expected phenology associated with budburst and chlorophyll biosynthesis in spring (from circa DOY 120) and chlorophyll breakdown during leaf senescence.

Temporal variations in cropland Chl_{Leaf} show a high variability globally, which is associated with different species of crops planted, planting regimes (i.e. single or double), fertiliser application and the level of irrigation. ENF temporal Chl_{Leaf} trajectories are relatively consistent across the year, although increasing Chl_{Leaf} within new needles in spring is detectible, along with some chlorophyll breakdown within winter months. Missing local data (predominately in the Amazon) within Figure 7a is due to too few original data points to generate standard deviation values. Importantly, Figure 7b demonstrates the temporal divergence of LAI and Chl_{Leaf} across the growing season, and a clear decoupling of vegetation structure and physiological function (Croft, Chen, and Zhang 2014b, Walther et al. 2016).

3.3 Spatial and biome-dependent trends

Annual maximum chlorophyll maps offer an opportunity to examine spatial differences in Chl_{Leaf} without the integration of a temporal bias from seasonal change. The geographic variability in the abundance of leaf chlorophyll depends in part on local environmental drivers, and partly on plant resource allocation.

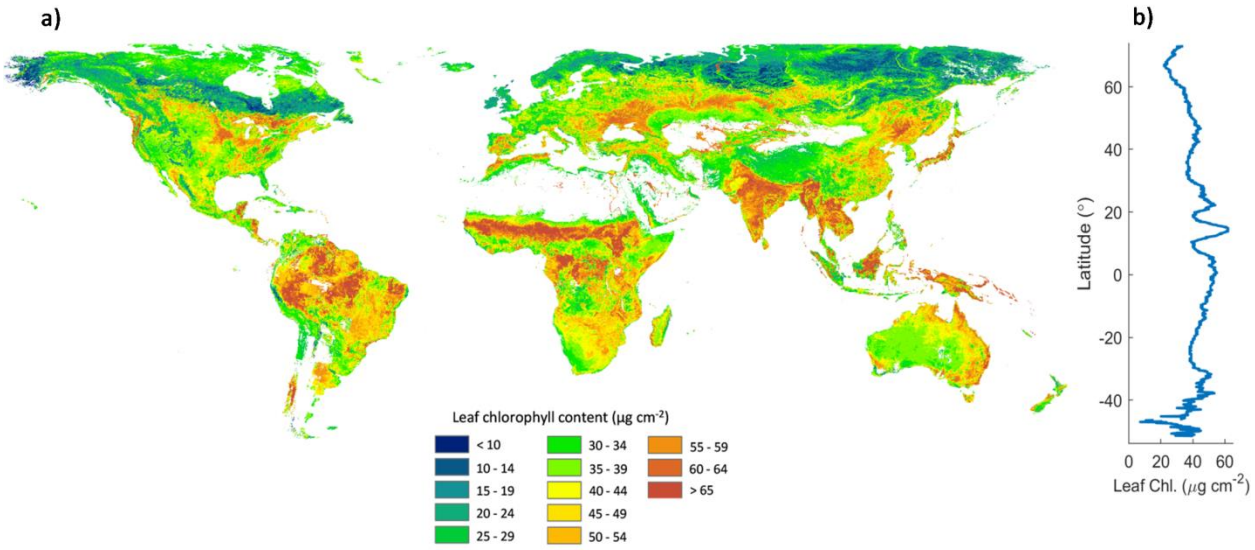

628

629

630 *Figure 8: a) Maximum annual leaf chlorophyll content (at 9 km resolution) and b) mean values of the*

631 *maximum along latitudinal bands.*

632

633 Higher annual maximum chlorophyll values (> 55 µg cm^{-2}) are associated with tropical forests and

634 croplands (Figure 8a). Mid-range values (25-55 µg cm^{-2}) are typical of grasslands, temperate broadleaf

635 forests and arctic tundra vegetation, and lower values (<25 µg cm^{-2}) are typical of boreal forests.

636 Considerable intra-biome chlorophyll variability also exists, for example within croplands higher annual

637 values are present in India, Eastern China, Western Europe and the great Lakes in USA/Canada, in

638 contrast to lower values found in Central Europe and the North American mid-west. Reasons for

639 chlorophyll variability over space are in part due to the abundance of elements needed for chlorophyll

640 synthesis (nitrogen (N), phosphorous (P), Magnesium (Mg)) (Li et al. 2018), which may vary due to the

641 nutrient availability status of the soil, the addition of fertilisers in managed landscapes and as a result of

642 atmospheric N deposition. At the biome-scale, the temperature-dependency of chlorophyll synthesis

643 reactions, where the optimum temperature of [3,8-DV]-Pchlide *a* 8-vinyl reductase (DVR) enzyme

644 activity in chlorophyll synthesis is 30°C (Nagata, Tanaka, and Tanaka 2007), may exert a biotic control on

the accumulation of chlorophyll in temperature-limiting ecosystems, such as the arctic. Additionally, plant water availability and drought stress affect the synthesis of chlorophyll, and may also prompt its accelerated breakdown (Ashraf and Harris 2013). As plants allocate resources to optimise physiological processes, it may be expected that solar irradiance conditions, and the leaf economics spectrum (Wright et al. 2004) affect the partitioning of nitrogen, both between and within structural and photosynthetic leaf fractions (Croft et al. 2017, Niinemets and Tenhunen 1997).

4.0 Sources of uncertainty in modelled leaf chlorophyll content

The validation results (Figure 5 and 6a) indicate a good algorithm performance and levels of uncertainty comparable to more local scale studies, with reported RMSE values in the literature ranging from around 8 to 15 μg cm^{-2} (Houborg et al. 2015). The uncertainties values from all of the PFTs used in this study were within this range; from GRS: 5.71 μg cm^{-2} through to EBF: 14.94 μg cm^{-2}, and the overall uncertainty of all PFTs considered together was 10.81 μg cm^{-2}. The overall uncertainty of the global Chl_{Leaf} product is therefore considered within reasonable limits of current state of the art approaches to chlorophyll modelling. The sources of uncertainty and future ways to minimise this uncertainty are discussed further below.

We highlight the main sources of uncertainty that can affect the accuracy of the modelled leaf chlorophyll values within the global maps as: 1) the data quality of the MERIS surface reflectance, 2) the accuracy of input LAI data, 3) the use of fixed structural parameters in canopy models, 4) the spectral contributions of understory or background reflectance to satellite-derived canopy reflectance, and 5) the validation sites used within the study.

1) Uncertainty in the MERIS surface reflectance product can arise from sources such as sensor calibration issues, cloud contamination, atmospheric correction errors (Garrigues et al. 2008). Due to the nature of the inversion process and the 'ill-posed problem' (Combal, Baret, and Weiss 2002), even small changes in satellite-derived reflectance can lead to large variations in modelled chlorophyll values (Garrigues et al. 2008).

2) The chlorophyll retrieval algorithm is strongly reliant on the LAI as an input parameter, where small errors in LAI values, particularly at low LAI values can lead to large errors in modelled chlorophyll. This introduces a greater uncertainty into the chlorophyll estimates in areas with little vegetation cover, for example in shrubland and deciduous plant forms at the start and end of the growing season. Errors in LAI at high LAI values, for example due to problems concerning reflectance saturation are less of a concern because the algorithm is less responsive to LAI > 4, or when the canopy behaves as a 'big leaf' and background and branch contributions are minimal. Clumping is considered in the GEOV1 LAI product that we selected (Baret et al., 2013), at both the landscape scale and the canopy scale through the integration of CYCLOPES v3.1 and MODIS c5 biophysical products. Errors in LAI values that arise from a lack of proper consideration of clumping effects mainly affect needleleaf canopies, which can be largely underestimated (Chen, Menges, and Leblanc 2005). The most significant problem, however, for the modelling of Chl_{Leaf} is a lack of accurate LAI during winter months in the northern hemisphere. The presence of snow on the understory and on the actual needleleaf shoots prevents the retrieval of LAI during large periods of time in the winter months. Any satellite-derived LAI data that is retrieved during snow-dominated winter months is highly uncertain, leading to potential problems with the smoothing algorithm. Further uncertainty arises from the LAI data product's coarser spatial resolution (1000 m), compared to the input MERIS surface reflectance product (300 m). The greatest uncertainty arising from this source will be in patchy or spatially variable landscapes, such as croplands or where the LAI values

692 are low (i.e. LAI = <3). This uncertainty will have less of a bearing on more spatially homogenous
693 landscapes (i.e. broadleaf forests) and in vegetation with higher LAI values.
694
695 3) The chlorophyll retrieval algorithm considers the major PFTs separately, through the application of
696 individual LUTs based on measured and reported ground data. However, the structural values used to
697 create the LUTs represent a generalised approximation of the structural parameters, and it is recognised
698 that considerable variation can exist within a given biome. An improved spatial representation of the
699 intra-PFT variability of structural parameters, such as canopy height, stem density and leaf angle
700 distribution, would be beneficial, particularly in needleleaf forests, for example, where spatial variability
701 is driven by the dominant species composition. However, a lack of available spatially-continuous data at
702 fine spatial resolutions currently prevents the explicit parameterisation of these structural variables in
703 the canopy models. Whilst these structural parameterisations are important, their variation over the
704 variable range that may be found within a PFT is likely to be small relative to variations between PFTs,
705 and relative to LAI. The sensitivity analysis presented in Section 2.4 indicates that LAI is the dominant
706 driver of modelled Chl_{Leaf} uncertainty, with other parameters such as crown height, ΩE, γE, Hs parameter
707 the background soil factor having negligible influence. This finding also confirms the work of Zhang et al.
708 (2008), who examined the sensitivity of the 4-Scale model input parameters to the model output,
709 finding that LAI is the dominant driver of modelled canopy reflectance.
710
711 4) The temporal and spatial variability of background contributions are a source of uncertainty in the
712 modelled Chl_{Leaf} values, to a greater or lesser degree depending on the overall canopy coverage. Areas
713 with lower LAI values are more susceptible to errors concerning the erroneous parameterisation of
714 background material in the model. Although substantial progress has been made in retrieving
715 understory reflectance from multi-angular reflectance images (Canisius and Chen 2007, Pisek and Chen

2009), the often coarse spatial resolution and lack of global coverage for all vegetation types of these products (Jiao et al. 2014, Liu et al. 2017) precludes their use.

5) An additional source of uncertainty could come from the validation ground data itself. The relatively small number of measured chlorophyll values sampled *in situ* makes widespread validation challenging, particularly for EBF, SHR and DNF PFTs. The validation data used in this study is through the generous and collaborative efforts of independent researchers, and without an established network collecting regular Chl_{Leaf} data or automated measurement systems, direct product validation is time and resource intensive (Garrigues et al. 2008). Consequently, no existing validation data sets are completely representative of all of the global and seasonal variability of vegetation [Baret et al., 2006]. This study used 28 distinct sites to validate the Chl_{Leaf} product, which is within the same range of other global biophysical product validations. In the calibration and product development of MODIS LAI products, Yang et al. (2006) selected 25 validation sites, and He et al (2012) used 38 validation sites for their 500 m global clumping index map. Initial Soil Moisture Active Passive (SMAP) soil moisture products were validated using 34 validation sites (Colliander et al. 2017). To an extent, the reported uncertainties on the modelled leaf chlorophyll content values will also be a function of the coverage of geographic and vegetation species contained within the validation sites, and the inherent variability that exists within plant functional types. Future work can focus on evaluating the accuracy of the chlorophyll product in species and management regimes that are underrepresented in the model development and validation. It is likely that sites where the structural properties deviate largest form the values used in the model parameterisation (Table 2) may suffer the largest degree of uncertainty.

5.0 Conclusion

This research represents the first global view of terrestrial Chl_{Leaf} distribution. Weekly maps of Chl_{Leaf} are produced at the global scale following a two-step physically-based modelling approach. The accuracy of the Chl_{Leaf} product is ultimately dependent on the representation of radiative transfer processes within the canopy and leaf optical models, the structural parameterisation of the radiative transfer models and the accuracy of land cover and leaf area index data. Modelled results show good relationships with measured ground data, in particular for deciduous broadleaf forests (R^2 = 0.67; RMSE = 9.25 µg cm^{-2}; p<0.001), croplands (R^2 = 0.41; RMSE = 13.18 µg cm^{-2}; p<0.001) and evergreen needleleaf forests (R^2 = 0.47; RMSE = 10.63 µg cm^{-2}; p<0.001). On an annual basis, evergreen broadleaf forests presented the highest median leaf chlorophyll values (54.4 µg cm^{-2}). The global values show large temporal and spatial variability expected in Chl_{Leaf}. It is expected that ESA Sentinel-2 series will be used to continue the Chl_{Leaf} time series, due to the presence of red-edge sampling bands and widespread spatial coverage and fine temporal resolution. It is anticipated that this global leaf chlorophyll product will make a significant step towards improving global and regional ecosystem models associated with carbon cycle modelling, through the explicit consideration of foliage biochemistry, and reduce the uncertainty associated with leaf physiology.

6.0 Acknowledgements

This work utilised data collected by grants funded by the Australian Research Council DP130101566. Beringer was funded under an ARC Future Fellowship (FT110100602). Support for OzFlux is provided through the Australia Terrestrial Ecosystem Research Network (TERN) (http://www.tern.org.au). Sele River Plain and Trapani data were collected by the University of Southampton for use in the MTCI-EVAL project and Demin data was collected as part of the AGRISAR 2006 ESA field campaign.

7.0 References

Amiri, Reza. 2013. "Hyperspectral remote sensing of vegetation - a transect approach." Ph.D, Monash University.

Arellano, Paul, Kevin Tansey, Heiko Balzter, and Doreen S Boyd. 2017. "Field spectroscopy and radiative transfer modelling to assess impacts of petroleum pollution on biophysical and biochemical parameters of the Amazon rainforest." *Environmental Earth Sciences* 76 (5):217.

Arellano, Paul, Kevin Tansey, Heiko Balzter, and Markus Tellkamp. 2017. "Plant Family-Specific Impacts of Petroleum Pollution on Biodiversity and Leaf Chlorophyll Content in the Amazon Rainforest of Ecuador." *PLOS ONE* 12 (1):e0169867. doi: 10.1371/journal.pone.0169867.

Ashraf, M., and P. J. C. Harris. 2013. "Photosynthesis under stressful environments: An overview." *Photosynthetica* 51 (2):163-190. doi: 10.1007/s11099-013-0021-6.

Asner, G. P., J. M. O. Scurlock, and J. A. Hicke. 2003. "Global synthesis of leaf area index observations: Implications for ecological and remote sensing studies." *Global Ecology and Biogeography* 12 (3):191-205.

Baret, F., M. Weiss, R. Lacaze, F. Camacho, H. Makhmara, P. Pacholcyzk, and B. Smets. 2013. "GEOV1: LAI and FAPAR essential climate variables and FCOVER global time series capitalizing over existing products. Part1: Principles of development and production." *Remote Sensing of Environment* 137:299-309. doi: http://dx.doi.org/10.1016/j.rse.2012.12.027.

Blackburn, G. A. 1998. "Quantifying chlorophylls and carotenoids at leaf and canopy scales: An evaluation of some hyperspectral approaches." *Remote Sensing of Environment* 66 (3):273-285.

Bonan, Gordon B, Peter J Lawrence, Keith W Oleson, Samuel Levis, Martin Jung, Markus Reichstein, David M Lawrence, and Sean C Swenson. 2011. "Improving canopy processes in the Community Land Model version 4 (CLM4) using global flux fields empirically inferred from FLUXNET data." *Journal of Geophysical Research: Biogeosciences (2005–2012)* 116 (G2).

Camacho, Fernando, Jesús Cernicharo, Roselyne Lacaze, Frédéric Baret, and Marie Weiss. 2013. "GEOV1: LAI, FAPAR essential climate variables and FCOVER global time series capitalizing over existing products. Part 2: Validation and intercomparison with reference products." *Remote Sensing of Environment* 137:310-329. doi: http://dx.doi.org/10.1016/j.rse.2013.02.030.

Canisius, Francis, and Jing M Chen. 2007. "Retrieving forest background reflectance in a boreal region from Multi-angle Imaging SpectroRadiometer (MISR) data." *Remote sensing of Environment* 107 (1):312-321.

Chen, J. M., and J. Cihlar. 1995. "Plant canopy gap-size analysis theory for improving optical measurements of leaf-area index." *Applied Optics* 34 (27):6211-6222.

Chen, J. M., and S. G. Leblanc. 1997. "A four-scale bidirectional reflectance model based on canopy architecture." *Geoscience and Remote Sensing, IEEE Transactions on* 35 (5):1316-1337.

Chen, J. M., and S. G. Leblanc. 2001. "Multiple-scattering scheme useful for geometric optical modeling." *Geoscience and Remote Sensing, IEEE Transactions on* 39 (5):1061-1071. doi: 10.1109/36.921424.

Chen, J. M., P. S. Plummer, M. Rich, S. T. Gower, and J. M. Norman. 1997. "Leaf area index of boreal forests: Theory, techniques and measurements." *Journal of Geophysical Research* 102 (D24):29-429.

Chen, Jing M, Feng Deng, and Mingzhen Chen. 2006. "Locally adjusted cubic-spline capping for reconstructing seasonal trajectories of a satellite-derived surface parameter." *IEEE Transactions on Geoscience and Remote Sensing* 44 (8):2230-2238.

Chen, JM, CH Menges, and SG Leblanc. 2005. "Global mapping of foliage clumping index using multi-angular satellite data." *Remote Sensing of Environment* 97 (4):447-457.

Chopping, Mark, Lihong Su, Albert Rango, John V Martonchik, Debra PC Peters, and Andrea Laliberte. 2008. "Remote sensing of woody shrub cover in desert grasslands using MISR with a geometric-optical canopy reflectance model." *Remote Sensing of Environment* 112 (1):19-34.

Clevers, Jan GPW, and Lammert Kooistra. 2012. "Using hyperspectral remote sensing data for retrieving canopy chlorophyll and nitrogen content." *IEEE Journal of Selected Topics in Applied Earth Observations and Remote Sensing* 5 (2):574-583.

Colliander, A, Thomas J Jackson, Rajat Bindlish, S Chan, N Das, SB Kim, MH Cosh, RS Dunbar, L Dang, and L Pashaian. 2017. "Validation of SMAP surface soil moisture products with core validation sites." *Remote Sensing of Environment* 191:215-231.

Combal, B., F. Baret, and M. Weiss. 2002. "Improving canopy variables estimation from remote sensing data by exploiting ancillary information. Case study on sugar beet canopies." *Agronomie* 22 (2):205-215.

Croft, H, JM Chen, NJ Froelich, B Chen, and RM Staebler. 2015. "Seasonal controls of canopy chlorophyll content on forest carbon uptake: Implications for GPP modeling." *Journal of Geophysical Research: Biogeosciences* 120 (8):1576-1586.

Croft, H, JM Chen, and TL Noland. 2014. "Stand age effects on Boreal forest physiology using a long time-series of satellite data." *Forest Ecology and Management* 328:202-208.

Croft, H, JM Chen, Y Zhang, A Simic, TL Noland, N Nesbitt, and J Arabian. 2015. "Evaluating leaf chlorophyll content prediction from multispectral remote sensing data within a physically-based modelling framework." *ISPRS Journal of Photogrammetry and Remote Sensing* 102:85-95.

Croft, H., and J. M. Chen. 2018. "Leaf Pigment Content." In *Comprehensive Remote Sensing*, edited by S. Liang, 117-142. Oxford: Elsevier.

Croft, H., J. M. Chen, X. Luo, P. Bartlett, B. Chen, and R. M. Staebler. 2017. "Leaf chlorophyll content as a proxy for leaf photosynthetic capacity." *Global Change Biology* 23 (9):1365-2486. doi: 10.1111/gcb.13599.

Croft, H., J. M. Chen, and Y. Zhang. 2014a. "The applicability of empirical vegetation indices for determining leaf chlorophyll content over different leaf and canopy structures." *Ecological Complexity* 17:119-130. doi: http://dx.doi.org/10.1016/j.ecocom.2013.11.005.

Croft, H., J. M. Chen, Y. Zhang, and A. Simic. 2013. "Modelling leaf chlorophyll content in broadleaf and needle leaf canopies from ground, CASI, Landsat TM 5 and MERIS reflectance data." *Remote Sensing of Environment* 133 (0):128-140. doi: http://dx.doi.org/10.1016/j.rse.2013.02.006.

Croft, H., J.M. Chen, and Y. Zhang. 2014b. "Temporal disparity in leaf chlorophyll content and leaf area index across a growing season in a temperate deciduous forest." *International Journal of Applied Earth Observation and Geoinformation* 33:312-320.

Curran, PJ, and CM Steele. 2005. "MERIS: The re-branding of an ocean sensor." *International Journal of Remote Sensing* 26 (9):1781-1798.

Darvishzadeh, Roshanak, Andrew Skidmore, Martin Schlerf, and Clement Atzberger. 2008. "Inversion of a radiative transfer model for estimating vegetation LAI and chlorophyll in a heterogeneous grassland." *Remote Sensing of Environment* 112 (5):2592-2604.

Datt, B. 1998. "Remote sensing of chlorophyll a, chlorophyll b, chlorophyll a+b, and total carotenoid content in eucalyptus leaves." *Remote Sensing of Environment* 66 (2):111-121.

De Santis, Angela, Emilio Chuvieco, and Patrick J Vaughan. 2009. "Short-term assessment of burn severity using the inversion of PROSPECT and GeoSail models." *Remote Sensing of Environment* 113 (1):126-136.

Demarez, V., and J. P. Gastellu-Etchegorry. 2000. "A modeling approach for studying forest chlorophyll content." *Remote Sensing of Environment* 71 (2):226-238.

856 Deng, F., J.M. Chen, S. Plummer, M. Chen, and J. Pisek. 2006. "Algorithm for global leaf area index
857 retrieval using satellite imagery." *IEEE Transactions on Geoscience and Remote Sensing* 44
858 (8):2219-2229. doi: 10.1109/TGRS.2006.872100.
859 Dong, Taifeng, Jiangui Liu, Budong Qian, Qi Jing, Holly Croft, Jingming Chen, Jinfei Wang, Ted Huffman,
860 Jiali Shang, and Pengfei Chen. 2017. "Deriving Maximum Light Use Efficiency From Crop Growth
861 Model and Satellite Data to Improve Crop Biomass Estimation." *IEEE Journal of Selected Topics*
862 *in Applied Earth Observations and Remote Sensing* 10 (1):104-117.
863 Enrique, G, Manuel Olmo, Hendrik Poorter, José Luis Ubera, and Rafael Villar. 2016. "Leaf mass per area
864 (LMA) and its relationship with leaf structure and anatomy in 34 Mediterranean woody species
865 along a water availability gradient." *PloS one* 11 (2):e0148788.
866 Evans, Matthew R., Aristides Moustakas, Gregory Carey, Yadvinder Malhi, Nathalie Butt, Sue Benham,
867 Denise Pallett, and Stefanie Schäfer. 2015. "Allometry and growth of eight tree taxa in United
868 Kingdom woodlands." *Scientific Data* 2:150006. doi: 10.1038/sdata.2015.6.
869 Feret, J. B., C. François, G. P. Asner, A. A. Gitelson, R. E. Martin, L. P. R. Bidel, S. L. Ustin, G. le Maire, and
870 S. Jacquemoud. 2008. "PROSPECT-4 and 5: Advances in the leaf optical properties model
871 separating photosynthetic pigments." *Remote Sensing of Environment* 112 (6):3030-3043.
872 Ferreira, Matheus P, Atilio E Grondona, Silvia Beatriz Alves Rolim, and Yosio E %J Journal of Applied
873 Remote Sensing Shimabukuro. 2013. "Analyzing the spectral variability of tropical tree species
874 using hyperspectral feature selection and leaf optical modeling." 7 (1):073502.
875 Féret, J. B., C. François, A. Gitelson, G. P. Asner, K. M. Barry, C. Panigada, A. D. Richardson, and S.
876 Jacquemoud. 2011. "Optimizing spectral indices and chemometric analysis of leaf chemical
877 properties using radiative transfer modeling." *Remote Sensing of Environment* 115 (10):2742-
878 2750.
879 Gamon, J. A., C. Coburn, L. B. Flanagan, K. F. Huemmrich, C. Kiddle, G. A. Sanchez-Azofeifa, D. R. Thayer,
880 L. Vescovo, D. Gianelle, and D. A. Sims. 2010. "SpecNet revisited: bridging flux and remote
881 sensing communities." *Canadian Journal of Remote Sensing* 36 (S2):376-390.
882 Garrigues, S., R. Lacaze, F. Baret, J. T. Morisette, M. Weiss, J. E. Nickeson, R. Fernandes, S. Plummer, N.
883 V. Shabanov, R. B. Myneni, Y. Knyazikhin, and W. Yang. 2008. "Validation and intercomparison of
884 global Leaf Area Index products derived from remote sensing data." *Journal of Geophysical*
885 *Research: Biogeosciences* 113 (G2):n/a-n/a. doi: 10.1029/2007JG000635.
886 Gastellu-Etchegorry, J. P., E. Martin, and F. Gascon. 2004. "DART: A 3D model for simulating satellite
887 images and studying surface radiation budget." *International Journal of Remote Sensing* 25
888 (1):73-96.
889 Gitelson, A. A., Y. Gritz, and M. N. Merzlyak. 2003. "Relationships between leaf chlorophyll content and
890 spectral reflectance and algorithms for non-destructive chlorophyll assessment in higher plant
891 leaves." *Journal of Plant Physiology* 160 (3):271-282.
892 Groenendijk, M., A. J. Dolman, M. K. van der Molen, R. Leuning, A. Arneth, N. Delpierre, J. H. C. Gash, A.
893 Lindroth, A. D. Richardson, H. Verbeeck, and G. Wohlfahrt. 2011. "Assessing parameter
894 variability in a photosynthesis model within and between plant functional types using global
895 Fluxnet eddy covariance data." *Agricultural and Forest Meteorology* 151 (1):22-38. doi:
896 http://dx.doi.org/10.1016/j.agrformet.2010.08.013.
897 Haboudane, D., J. R. Miller, N. Tremblay, P. J. Zarco-Tejada, and L. Dextraze. 2002. "Integrated narrow-
898 band vegetation indices for prediction of crop chlorophyll content for application to precision
899 agriculture." *Remote Sensing of Environment* 81 (2-3):416-426.
900 Hajnsek, I, R Bianchi, M Davidson, and M Wooding. 2006. "AgriSAR 2006—Airborne SAR and optics
901 campaigns for an improved monitoring of agricultural processes and practices." Proc. AgriSAR
902 Workshop.

He, Liming, Jing M Chen, Jan Pisek, Crystal B Schaaf, and Alan H Strahler. 2012. "Global clumping index map derived from the MODIS BRDF product." *Remote Sensing of Environment* 119:118-130.

He, Liming, Jing M. Chen, Holly Croft, Alemu Gonsamo, Xiangzhong Luo, Jane Liu, Ting Zheng, Ronggao Liu, and Yang Liu. 2017. "Nitrogen Availability Dampens the Positive Impacts of CO2 Fertilization on Terrestrial Ecosystem Carbon and Water Cycles." *Geophysical Research Letters* 44 (22):11,590-11,600. doi: 10.1002/2017GL075981.

He, Liming, Jane Liu, Jing M. Chen, Holly Croft, Rong Wang, Michael Sprintsin, Ting Zheng, Youngryel Ryu, Jan Pisek, Alemu Gonsamo, Feng Deng, and Yongqin Zhang. 2016. "Inter- and intra-annual variations of clumping index derived from the MODIS BRDF product." *International Journal of Applied Earth Observation and Geoinformation* 44:53-60. doi: https://doi.org/10.1016/j.jag.2015.07.007.

He, Yuhong, Xulin Guo, and John F Wilmshurst. 2007. "Comparison of different methods for measuring leaf area index in a mixed grassland." *Canadian Journal of Plant Science* 87 (4):803-813.

Homolová, L, ME Schaepman, P Lamarque, JGPW Clevers, F de Bello, W Thuiller, and S Lavorel. 2014. "Comparison of remote sensing and plant trait-based modelling to predict ecosystem services in subalpine grasslands." *Ecosphere* 5 (8):1-29.

Homolová, Lucie, Petr Lukeš, Zbyněk Malenovský, Zuzana Lhotáková, Věroslav Kaplan, and Jan Hanuš. 2013. "Measurement methods and variability assessment of the Norway spruce total leaf area: implications for remote sensing." *Trees* 27 (1):111-121.

Homolová, Lucie, Zbyněk Malenovský, Jan GPW Clevers, Glenda Garcia-Santos, and Michael E Schaepman. 2013. "Review of optical-based remote sensing for plant trait mapping." *Ecological Complexity* 15:1-16.

Hosgood, B., S. Jacquemoud, G. Andreoli, J. Verdebout, G. Pedrini, and G. Schmuck. 1995. "Leaf Optical Properties Experiment 93 (LOPEX93)." *European Commission, Joint Research Centre, Institute for Remote Sensing Applications, Report EUR 16095 EN*.

Houborg, R., and E. Boegh. 2008. "Mapping leaf chlorophyll and leaf area index using inverse and forward canopy reflectance modeling and SPOT reflectance data." *Remote sensing of environment* 112 (1):186-202.

Houborg, Rasmus, Matthew McCabe, Alessandro Cescatti, Feng Gao, Mitchell Schull, and Anatoly Gitelson. 2015. "Joint leaf chlorophyll content and leaf area index retrieval from Landsat data using a regularized model inversion system (REGFLEC)." *Remote Sensing of Environment* 159 (Supplement C):203-221. doi: https://doi.org/10.1016/j.rse.2014.12.008.

Huemmrich, K. F. 2001. "The GeoSail model: a simple addition to the SAIL model to describe discontinuous canopy reflectance." *Remote Sensing of Environment* 75 (3):423-431. doi: http://dx.doi.org/10.1016/S0034-4257(00)00184-X.

Jacquemoud, S., C. Bacour, H. Poilvé, and J. P. Frangi. 2000. "Comparison of four radiative transfer models to simulate plant canopies reflectance: Direct and inverse mode." *Remote Sensing of Environment* 74 (3):471-481.

Jacquemoud, S., and F. Baret. 1990. "PROSPECT: A model of leaf optical properties spectra." *Remote Sensing of Environment* 34 (2):75-91.

Jacquemoud, Stéphane, Wout Verhoef, Frédéric Baret, Cédric Bacour, Pablo J Zarco-Tejada, Gregory P Asner, Christophe François, and Susan L Ustin. 2009. "PROSPECT+ SAIL models: A review of use for vegetation characterization." *Remote sensing of environment* 113:S56-S66.

Jiao, Tong, Ronggao Liu, Yang Liu, Jan Pisek, and Jing M. Chen. 2014. "Mapping global seasonal forest background reflectivity with Multi-angle Imaging Spectroradiometer data." *Journal of Geophysical Research: Biogeosciences* 119 (6):1063-1077. doi: 10.1002/2013JG002493.

Kempeneers, P., P. J. Zarco-Tejada, P. R. J. North, S. de Backer, S. Delalieux, G. Sepulcre-Cantó, F. Morales, J. A. N. van Aardt, R. Sagardoy, P. Coppin, and P. Scheunders. 2008. "Model inversion

951 for chlorophyll estimation in open canopies from hyperspectral imagery." *International Journal*
952 *of Remote Sensing* 29 (17-18):5093-5111. doi: 10.1080/01431160802036458.
953 Knyazikhin, Y., J. V. Martonchik, R. B. Myneni, D. J. Diner, and S. W. Running. 1998. "Synergistic
954 algorithm for estimating vegetation canopy leaf area index and fraction of absorbed
955 photosynthetically active radiation from MODIS and MISR data." *Journal of Geophysical*
956 *Research D: Atmospheres* 103 (D24):32257-32275.
957 Kötz, Benjamin, Michael Schaepman, Felix Morsdorf, Paul Bowyer, Klaus Itten, and Britta Allgöwer. 2004.
958 "Radiative transfer modeling within a heterogeneous canopy for estimation of forest fire fuel
959 properties." *Remote Sensing of Environment* 92 (3):332-344.
960 Le Maire, G., C. François, and E. Dufrêne. 2004. "Towards universal broad leaf chlorophyll indices using
961 PROSPECT simulated database and hyperspectral reflectance measurements." *Remote Sensing*
962 *of Environment* 89 (1):1-28.
963 Leblanc, S.G., P. Bicheron, J.M. Chen, M. Leroy, and J. Cihlar. 1999. "Investigation of directional
964 reflectance in boreal forests with an improved four-scale model and airborne POLDER data."
965 *IEEE Transactions on Geoscience and Remote Sensing* 37 (3):1396-1414. doi: 10.1109/36.763304.
966 Li, Ying, Nianpeng He, Jihua Hou, Li Xu, Congcong Liu, Jiahui Zhang, Qiufeng Wang, Ximin Zhang, and
967 Xiuqin Wu. 2018. "Factors influencing leaf chlorophyll content in natural forests at the biome
968 scale." *Frontiers in Ecology and Evolution* 6:64.
969 Liu, Jiangui, Elizabeth Pattey, and Guillaume Jégo. 2012. "Assessment of vegetation indices for regional
970 crop green LAI estimation from Landsat images over multiple growing seasons." *Remote Sensing*
971 *of Environment* 123:347-358.
972 Liu, Yang, Ronggao Liu, Jan Pisek, and Jing M Chen. 2017. "Separating of Overstory and Understory Leaf
973 Area Indices for Global Needleleaf and Deciduous Broadleaf Forests by Fusion of MODIS and
974 MISR Data." *Biogeosciences*.
975 Los, SO, J Rosette, Natascha Kljun, PRJ North, Laura Chasmer, J Suárez, Chris Hopkinson, RA Hill, Eva Van
976 Gorsel, and Craig Mahoney. 2012. "Vegetation height products between 60° S and 60° N from
977 ICESat GLAS data." *Geoscientific Model Development* 5:413-432.
978 Luo, Xiangzhong, Holly Croft, Jing M. Chen, Paul Bartlett, Ralf Staebler, and Norma Froelich. 2018.
979 "Incorporating leaf chlorophyll content into a two-leaf terrestrial biosphere model for
980 estimating carbon and water fluxes at a forest site." *Agricultural and Forest Meteorology* 248
981 (Supplement C):156-168. doi: https://doi.org/10.1016/j.agrformet.2017.09.012.
982 Malenovský, Z, J Albrechtová, Z Lhotáková, R Zurita-Milla, JGPW Clevers, ME Schaepman, and P Cudlín.
983 2006. "Applicability of the PROSPECT model for Norway spruce needles." *International Journal*
984 *of Remote Sensing* 27 (24):5315-5340.
985 Malenovský, Z., E. Martin, L. Homolová, J. P. Gastellu-Etchegorry, R. Zurita-Milla, M. E. Schaepman, R.
986 Pokorný, J. G. P. W. Clevers, and P. Cudlín. 2008. "Influence of woody elements of a Norway
987 spruce canopy on nadir reflectance simulated by the DART model at very high spatial
988 resolution." *Remote Sensing of Environment* 112 (1):1-18.
989 Malenovský, Zbyněk, Lucie Homolová, Raúl Zurita-Milla, Petr Lukeš, Věroslav Kaplan, Jan Hanuš, Jean-
990 Philippe Gastellu-Etchegorry, and Michael E Schaepman. 2013. "Retrieval of spruce leaf
991 chlorophyll content from airborne image data using continuum removal and radiative transfer."
992 *Remote Sensing of Environment* 131:85-102.
993 McGinn, Sean M. 2010. "Weather and climate patterns in Canada's prairie grasslands." *Arthropods of*
994 *Canadian grasslands* 1:105-119.
995 Middleton, EM, JH Sullivan, BD Bovard, AJ Deluca, SS Chan, and TA Cannon. 1997. "Seasonal variability in
996 foliar characteristics and physiology for boreal forest species at the five Saskatchewan tower
997 sites during the 1994 Boreal Ecosystem-Atmosphere Study." *Journal of Geophysical Research:*
998 *Atmospheres* 102 (D24):28831-28844.

Migliavacca, Mirco, Oscar Perez-Priego, Micol Rossini, Tarek S El-Madany, Gerardo Moreno, Christiaan van der Tol, Uwe Rascher, Anna Berninger, Verena Bessenbacher, and Andreas Burkart. 2017. "Plant functional traits and canopy structure control the relationship between photosynthetic CO 2 uptake and far-red sun-induced fluorescence in a Mediterranean grassland under different nutrient availability." *New Phytologist* 214 (3):1078-1091.

Moorthy, I., J. R. Miller, and T. L. Noland. 2008. "Estimating chlorophyll concentration in conifer needles with hyperspectral data: An assessment at the needle and canopy level." *Remote Sensing of Environment* 112 (6):2824-2838.

Mutanga, O., and A. K. Skidmore. 2004. "Hyperspectral band depth analysis for a better estimation of grass biomass (Cenchrus ciliaris) measured under controlled laboratory conditions." *International Journal of Applied Earth Observation and Geoinformation* 5 (2):87-96.

Nagata, Nozomi, Ryouichi Tanaka, and Ayumi Tanaka. 2007. "The major route for chlorophyll synthesis includes [3, 8-divinyl]-chlorophyllide a reduction in Arabidopsis thaliana." *Plant and cell physiology* 48 (12):1803-1808.

Niinemets, Ü, and J. D. Tenhunen. 1997. "A model separating leaf structural and physiological effects on carbon gain along light gradients for the shade-tolerant species Acer saccharum." *Plant, Cell and Environment* 20 (7):845-866.

North, P. 1996. "Three-dimensional forest light interaction model using a Monte Carlo method." *Geoscience and Remote Sensing, IEEE Transactions on* 34 (4):946-956. doi: 10.1109/36.508411.

Peng, Y., A. A. Gitelson, G. Keydan, D. C. Rundquist, and W. Moses. 2011. "Remote estimation of gross primary production in maize and support for a new paradigm based on total crop chlorophyll content." *Remote Sensing of Environment* 115 (4):978-989.

Peng, Yi, Anthony Nguy-Robertson, Timothy Arkebauer, and Anatoly Gitelson. 2017. "Assessment of canopy chlorophyll content retrieval in maize and soybean: implications of hysteresis on the development of generic algorithms." *Remote Sensing* 9 (3):226.

Pisek, Jan, and Jing M Chen. 2009. "Mapping forest background reflectivity over North America with Multi-angle Imaging SpectroRadiometer (MISR) data." *Remote Sensing of Environment* 113 (11):2412-2423.

Pisek, Jan, Jing Ming Chen, and Tiit Nilson. 2011. "Estimation of vegetation clumping index using MODIS BRDF data." *International Journal of Remote Sensing* 32 (9):2645-2657.

Porcar-Castell, Albert, Esa Tyystjärvi, Jon Atherton, Christiaan van der Tol, Jaume Flexas, Erhard E Pfündel, Jose Moreno, Christian Frankenberg, and Joseph A Berry. 2014. "Linking chlorophyll a fluorescence to photosynthesis for remote sensing applications: mechanisms and challenges." *Journal of experimental botany*:eru191.

Pottier, Julien, Zbyněk Malenovský, Achilleas Psomas, Lucie Homolová, Michael E. Schaepman, Philippe Choler, Wilfried Thuiller, Antoine Guisan, and Niklaus E. Zimmermann. 2014. "Modelling plant species distribution in alpine grasslands using airborne imaging spectroscopy." *Biology Letters* 10 (7). doi: 10.1098/rsbl.2014.0347.

Privette, Jeffrey L, Ranga B Myneni, William J Emery, and Forrest G Hall. 1996. "Optimal sampling conditions for estimating grassland parameters via reflectance." *IEEE Transactions on Geoscience and Remote Sensing* 34 (1):272-284.

Roberts, Dar A, Keely L Roth, and Ryan L Perroy. 2016. "Hyperspectral vegetation indices." In *Hyperspectral remote sensing of vegetation.*, edited by J.G. Lyon P.S. Thenkabail, and A. Huete, 309. Taylor and Francis.

Rowland, Lucy, Timothy Charles Hill, Clement Stahl, Lukas Siebicke, Benoit Burban, Joana Zaragoza-Castells, Stephane Ponton, Damien Bonal, Patrick Meir, and Mathew Williams. 2014. "Evidence for strong seasonality in the carbon storage and carbon use efficiency of an Amazonian forest." *Global change biology* 20 (3):979-991.

1047 Sandmeier, Stefan R, Elizabeth M Middleton, Donald W Deering, and Wenhan Qin. 1999. "The potential
1048 of hyperspectral bidirectional reflectance distribution function data for grass canopy
1049 characterization." *Journal of Geophysical Research: Atmospheres* 104 (D8):9547-9560.
1050 Serrano, L. 2008. "Effects of leaf structure on reflectance estimates of chlorophyll content."
1051 *International Journal of Remote Sensing* 29 (17-18):5265-5274.
1052 Simic, A., J. M. Chen, and T. L. Noland. 2011. "Retrieval of forest chlorophyll content using canopy
1053 structure parameters derived from multi-angle data: the measurement concept of combining
1054 nadir hyperspectral and off-nadir multispectral data." *International Journal of Remote Sensing*
1055 32 (20):5621-5644.
1056 Sims, D. A., and J. A. Gamon. 2002. "Relationships between leaf pigment content and spectral
1057 reflectance across a wide range of species, leaf structures and developmental stages." *Remote*
1058 *Sensing of Environment* 81 (2-3):337-354.
1059 Sow, Momadou, Cheikh Mbow, Christelle Hély, Rasmus Fensholt, and Bienvenu Sambou. 2013.
1060 "Estimation of herbaceous fuel moisture content using vegetation indices and land surface
1061 temperature from MODIS data." *Remote Sensing* 5 (6):2617-2638.
1062 Suits, Gwynn H. 1971. "The calculation of the directional reflectance of a vegetative canopy." *Remote*
1063 *Sensing of Environment* 2:117-125.
1064 Thorpe, H. C., R. Astrup, A. Trowbridge, and K. D. Coates. 2010. "Competition and tree crowns: A
1065 neighborhood analysis of three boreal tree species." *Forest Ecology and Management* 259
1066 (8):1586-1596. doi: https://doi.org/10.1016/j.foreco.2010.01.035.
1067 Tong, Alexander, and Yuhong He. 2017. "Estimating and mapping chlorophyll content for a
1068 heterogeneous grassland: Comparing prediction power of a suite of vegetation indices across
1069 scales between years." *ISPRS Journal of Photogrammetry and Remote Sensing* 126:146-167.
1070 Tum, Markus, Kurt Günther, Martin Böttcher, Frédéric Baret, Michael Bittner, Carsten Brockmann, and
1071 Marie Weiss. 2016. "Global Gap-Free MERIS LAI Time Series (2002–2012)." *Remote Sensing* 8
1072 (1):69.
1073 Verger, Aleixandre, Frédéric Baret, Marie Weiss, Iolanda Filella, and Josep Peñuelas. 2015. "GEOCLIM: A
1074 global climatology of LAI, FAPAR, and FCOVER from VEGETATION observations for 1999–2010."
1075 *Remote Sensing of Environment* 166:126-137. doi: http://dx.doi.org/10.1016/j.rse.2015.05.027.
1076 Verhoef, W. 1984. "Light scattering by leaf layers with application to canopy reflectance modeling: The
1077 SAIL model." *Remote Sensing of Environment* 16 (2):125-141.
1078 Verhoef, W. 1985. "Earth observation modeling based on layer scattering matrices." *Remote Sensing of*
1079 *Environment* 17 (2):165-178.
1080 Verma, Manish, David Schimel, Bradley Evans, Christian Frankenberg, Jason Beringer, Darren T Drewry,
1081 Troy Magney, Ian Marang, Lindsay Hutley, and Caitlin Moore. 2017. "Effect of environmental
1082 conditions on the relationship between solar-induced fluorescence and gross primary
1083 productivity at an OzFlux grassland site." *Journal of Geophysical Research: Biogeosciences* 122
1084 (3):716-733.
1085 Verrelst, Jochem, Michael E Schaepman, Zbyněk Malenovský, and Jan GPW Clevers. 2010. "Effects of
1086 woody elements on simulated canopy reflectance: Implications for forest chlorophyll content
1087 retrieval." *Remote Sensing of Environment* 114 (3):647-656.
1088 Vohland, M., and T. Jarmer. 2008. "Estimating structural and biochemical parameters for grassland from
1089 spectroradiometer data by radiative transfer modelling (PROSPECT+SAIL)." *International Journal*
1090 *of Remote Sensing* 29 (1):191-209. doi: 10.1080/01431160701268947.
1091 Vuolo, Francesco, Jadunandan Dash, Paul J Curran, Dulce Lajas, and Ewa Kwiatkowska. 2012.
1092 "Methodologies and uncertainties in the use of the terrestrial chlorophyll index for the Sentinel-
1093 3 mission." *Remote Sensing* 4 (5):1112-1133.

Walther, Sophia, Maximilian Voigt, Tea Thum, Alemu Gonsamo, Yongguang Zhang, Philipp Köhler, Martin Jung, Andrej Varlagin, and Luis Guanter. 2016. "Satellite chlorophyll fluorescence measurements reveal large-scale decoupling of photosynthesis and greenness dynamics in boreal evergreen forests." *Global change biology* 22 (9):2979-2996.

Wright, I. J., P. B. Reich, M. Westoby, D. D. Ackerly, Z. Baruch, F. Bongers, J. Cavender-Bares, T. Chapin, J. H. C. Cornellssen, M. Diemer, J. Flexas, E. Garnier, P. K. Groom, J. Gulias, K. Hikosaka, B. B. Lamont, T. Lee, W. Lee, C. Lusk, J. J. Midgley, M. L. Navas, Ü Niinemets, J. Oleksyn, H. Osada, H. Poorter, P. Pool, L. Prior, V. I. Pyankov, C. Roumet, S. C. Thomas, M. G. Tjoelker, E. J. Veneklaas, and R. Villar. 2004. "The worldwide leaf economics spectrum." *Nature* 428 (6985):821-827.

Yang, Wenze, Bin Tan, Dong Huang, Miina Rautiainen, Nikolay V Shabanov, Yujie Wang, Jeffrey L Privette, Karl Fred Huemmrich, Rasmus Fensholt, and Inge Sandholt. 2006. "MODIS leaf area index products: From validation to algorithm improvement." *IEEE Transactions on Geoscience and Remote Sensing* 44 (7):1885-1898.

Yi, Qiuxiang, Guli Jiapaer, Jingming Chen, Anming Bao, and Fumin Wang. 2014. "Different units of measurement of carotenoids estimation in cotton using hyperspectral indices and partial least square regression." *ISPRS Journal of Photogrammetry and Remote Sensing* 91:72-84.

Zarco-Tejada, P. J., J. R. Miller, J. Harron, B. Hu, T. L. Noland, N. Goel, G. H. Mohammed, and P. Sampson. 2004. "Needle chlorophyll content estimation through model inversion using hyperspectral data from boreal conifer forest canopies." *Remote Sensing of Environment* 89 (2):189-199.

Zarco-Tejada, P. J., J. R. Miller, T. L. Noland, G. H. Mohammed, and P. H. Sampson. 2001. "Scaling-up and model inversion methods with narrowband optical indices for chlorophyll content estimation in closed forest canopies with hyperspectral data." *IEEE Transactions on Geoscience and Remote Sensing* 39 (7):1491-1507.

Zhang, Y., J. M. Chen, J. R. Miller, and T. L. Noland. 2008. "Leaf chlorophyll content retrieval from airborne hyperspectral remote sensing imagery." *Remote Sensing of Environment* 112 (7):3234-3247.

Zhang, Y., J. M. Chen, and S. C. Thomas. 2007. "Retrieving seasonal variation in chlorophyll content of overstory and understory sugar maple leaves from leaf-level hyperspectral data." *Canadian Journal of Remote Sensing* 33 (5):406-415.

Zou, Xiaochen, and Matti Mõttus. 2015. "Retrieving crop leaf tilt angle from imaging spectroscopy data." *Agricultural and Forest Meteorology* 205:73-82.